



TECHNISCHE
UNIVERSITÄT
WIEN

Master Thesis

Hantzsch Esters as Formylation Agents under Photochemical Conditions

Conducted at the

Institute of Applied Synthetic Chemistry (TU Wien)

and the

Institute of Inorganic and Applied Chemistry (Universität Hamburg)

under the supervision of

Univ. Prof. Dipl.-Ing. Dr. techn. Katharina Schröder

by

Dorottya Mikoczi, BSc

Matrikelnr.: 01326573

Vienna, February 2024

DANKSAGUNG

Ich möchte mich bei allen Personen bedanken, die mich während meines Studiums unterstützt haben.

Ein besonderer Dank gilt Prof. Katharina Schröder für ihre Unterstützung und *Ádám Pálvölgyi*, der die Idee hatte, eine andere Forschungsgruppe auszuprobieren und mich in Hamburg zu bewerben.

Bei Prof. Axel Jacobi von Wangelin möchte ich mich für seine Betreuung bedanken und auch Mattis Schmotz für seine kontinuierliche Unterstützung und Ideen zu meinem Thema. Ich war sehr dankbar für die Möglichkeit, ein Auslandssemester in Hamburg zu absolvieren, und für die äußerst freundliche Gruppe, die mich empfangen hat. Es war eine großartige Erfahrung.

Und vor allem möchte ich mich bei meinen Eltern bedanken. Ohne ihre kontinuierliche Unterstützung wäre ich heute nicht hier. Und auch ein Dankeschön an Dani, der immer für mich da ist.

TABLE OF CONTENTS

Danksagung	II
Table of Contents	III
Abstract	VI
Kurzfassung	VII
Abbreviations	VIII
1 Introduction	1
1.1 Basics of photochemistry.....	1
1.2 Jablonski diagram.....	2
1.3 Thermal and photochemical reactions	4
1.4 Photoredox reactions.....	6
1.5 Photochemical strategies.....	9
1.5.1 Photoredox catalysis.....	10
1.5.2 Direct photoexcitation of reaction substrates	11
1.5.3 EDA complex formation	12
1.6 Hantzsch esters	13
2 Aim of the thesis	16
3 Results and Discussion	19
3.1 Hantzsch ester synthesis.....	19
3.2 Photoreaction design	22
3.2.1 Investigations of the UV-VIS absorption properties	22
3.2.1.1 UV-VIS absorption of the Hantzsch ester (HE 2).....	22
3.2.1.2 UV-VIS absorption of the reaction mixture	23
3.2.2 Optimization of the reaction conditions	24
3.2.3 Reaction setup	26

3.3	Reaction development	30
3.3.1	Substrate scope	30
3.4	Mechanistic investigations	33
3.4.1	Characterization of the ground state	33
3.4.2	Characterization of the excited state	35
3.4.3	Characterization of reaction intermediates	37
3.4.3.1	Radical trapping experiment	37
3.4.3.2	Light on/off experiment	39
3.4.4	Plausible reaction pathway	40
4	Conclusion and Outlook	41
5	Experimental section	42
5.1	Materials and methods	42
5.2	Synthesis of Hantzsch esters	44
5.2.1	Synthesis of Diethyl 4-(dimethoxymethyl)-2,6-dimethyl-1,4-dihydropyridine-3,5-dicarboxylate (HE 1)	44
5.2.2	Synthesis of Diethyl 4-(1,3-dithian-2-yl)-2,6-dimethyl-1,4-dihydropyridine-3,5-dicarboxylate (HE 2)	45
5.2.2.1	Method 1	45
5.2.2.2	Method 2	46
5.2.3	Unsuccessful synthesis of HE 2	47
5.2.3.1	Synthesis of 2-Formyl-1,3-dithiane (P 1)	47
5.2.3.2	Synthesis of Ethyl 3-(1,3-dithian-2-ylidene)propanoate (P 3)	48
5.3	Acetalization of olefines under photochemical conditions	49
5.4	General procedures	49
5.4.1	General procedure A	49
5.4.2	General procedure B	50
5.4.3	General procedure C	51

5.5	Isolated compounds.....	52
5.5.1	2-((1,3-Dithian-2-yl)(phenyl)methyl)malononitrile (1b).....	52
5.5.2	2-(2,2-Dimethoxy-1-phenylethyl)malononitrile (1a).....	52
5.5.3	2-(2,2-Dimethoxy-1-(3-methoxyphenyl)ethyl) malononitrile (2a).....	53
5.5.4	2-(2,2-Dimethoxy-1-(4-methoxyphenyl)ethyl) malononitrile (3a).....	53
5.5.5	2-(1-(3-Hydroxyphenyl)-2,2-dimethoxyethyl) malononitrile (4a).....	54
5.5.6	2-(1-(2-Fluorophenyl)-2,2-dimethoxyethyl) malononitrile (5a).....	54
5.5.7	2-(1-(3-Chlorophenyl)-2,2-dimethoxyethyl) malononitrile (6a).....	55
5.5.8	2-(1-(3-Bromophenyl)-2,2-dimethoxyethyl) malononitrile (7a).....	55
5.5.9	2-(1-(4-Iodophenyl)-2,2-dimethoxyethyl)malononitrile (8a).....	56
5.5.10	2-(2,2-Dimethoxy-1-(3-(4,4,5,5-tetramethyl-1,3,2-dioxaborolan-2-yl)phenyl)ethyl) malononitrile (9a).....	56
5.5.11	2-(1-(4-Ethynylphenyl)-2,2-dimethoxyethyl) malononitrile (10a).....	57
5.5.12	2-(2,2-Dimethoxy-1-(4-(methylthio)phenyl)ethyl) malononitrile (11a)....	57
5.5.13	2-(2,2-Dimethoxy-1-(3-((triisopropylsilyl)oxy)phenyl)ethyl)malononitrile (12a).....	58
5.5.14	2-(2,2-Dimethoxy-1-(3-methyl-1-phenyl-1 <i>H</i> -pyrazol-4-yl)ethyl)malononitrile (13a).....	58
5.5.15	2-(2,2-Dimethoxy-1-(5-methylfuran-2-yl)ethyl) malononitrile (14a).....	59
5.5.16	2-(2,2-Dimethoxy-1-(thiophen-2-yl)ethyl) malononitrile (15a).....	59
5.5.17	2-(1-Cyclohexyl-2,2-dimethoxyethyl) malononitrile (16a).....	60
5.5.18	2-(1,1-Dimethoxy-2-phenylpropan-2-yl) malononitrile (17a).....	60
5.5.19	Diethyl 2-(2,2-dimethoxy-1-phenylethyl) malonate (18a).....	61
6	List of figures	62
7	List of tables	64
8	References.....	65

ABSTRACT

Photoreactions have gained prominence due to their ability to operate under mild conditions, aligning with the principles of green chemistry. Hantzsch esters have gained recognition as significant compounds for their role as hydrogen donors in transfer reactions. In recent developments, excited Hantzsch esters have been recognized as potent reductants, opening new avenues for the application in radical reactions and expanding their role as efficient radical reservoirs for late-stage functionalization.

This thesis focuses on the formation of acetals from activated olefins employing Hantzsch esters both as reducing agents and acetal reservoirs. This approach not only aligns with the principles of green chemistry but also expands the repertoire of strategies for late-stage functionalization. Investigations into different parameters were undertaken to determine the optimal reaction conditions, leading to an expanded scope that encompasses a variety of olefins. The newly established system exhibited consistently high yields across a broad range of substrates.

KURZFASSUNG

Photoreaktionen haben an Bedeutung gewonnen, da sie unter milden Bedingungen durchführbar sind und somit den Prinzipien der grünen Chemie entsprechen. Hantzsch-Ester sind bereits als Wasserstoff-Donoren in Transferreaktionen etabliert. In neusten Entwicklungen wurden angeregte Hantzsch-Ester als starke Reduktionsmittel identifiziert, die neue Anwendungsmöglichkeiten in radikalischen Reaktionen eröffnen und als effiziente Radikal-Reservoirs für die Funktionalisierung in fortgeschrittenen Stadien agieren.

Diese Arbeit konzentriert sich auf die Synthese von Acetalen aus aktivierten Olefinen unter Verwendung von Hantzsch-Estern sowohl als Reduktionsmittel als auch als Acetal-Reservoirs. Dieser innovative Ansatz entspricht nicht nur den Prinzipien der grünen Chemie, sondern erweitert auch das Repertoire von Strategien zur Funktionalisierung komplexer Moleküle in fortgeschrittenen Stadien. Untersuchungen zu verschiedenen Parametern wurden durchgeführt, um die optimalen Reaktionsbedingungen für verschiedene Olefine mit erweitertem Anwendungsbereich zu entwickeln. Das neu etablierte System zeigte durchweg hohe Ausbeuten für ein breites Spektrum von Substraten.

ABBREVIATIONS

3DPA2FBN	2,4,6-Tris(diphenylamino)-3,5-difluorobenzonitrile
4CzIPN	1,2,3,5-Tetrakis(carbazol-9-yl)-4,6-dicyanobenzene
a.u.	Absorbance unit
Alox N	Aluminium oxide, neutral
ATH	Asymmetric transfer hydrogenation
BF ₃ -Et ₂ O	Boron trifluoride diethyl etherate
DCM	Methylene chloride
DMI	1,3-Dimethyl-2-imidazolidinone
EDA	Electron-donor-acceptor
EtOAc	Ethyl acetate
EWG	Electron withdrawing group
HAT	Hydrogen atom transfer
HE	Hantzsch ester
HOMO	Highest occupied molecular orbital
LUMO	Lowest unoccupied molecular orbital
MeCN	Acetonitrile
MeOH	Methanol
NAD	Nicotinamide adenine dinucleotide
NADP	Nicotinamide adenine dinucleotide phosphate
PC	Photocatalyst
PET	Photoinduced electron transfer
SET	Single electron transfer
TEMPO	(2,2,6,6-Tetramethylpiperidin-1-yl)oxyl
THF	Tetrahydrofuran
TLC	Thin layer chromatography

1 INTRODUCTION

Photochemistry plays a key role in Earth's history.^[1] The most essential photochemical reaction is indisputably the photosynthesis, which is the source of all our food and most of our energy resources.^[2] Despite the fact that some photochemical processes are ancient, synthetic photochemistry have attracted systematic scientific investigations only relatively recently.^[3]

Photochemistry in organic synthesis evolved only slowly over the past 100 years, but this is bound to change with the increasing focus on green chemistry. Green chemistry and photocatalysis are two of the most rapidly emerging research directions in organic chemistry of the last 10 years based on publication trend analysis.^[4] The ability to address the rising problem of global warming also requires more efficient and environmentally friendly chemical processes, which justifies the growing interest in these research fields.

1.1 BASICS OF PHOTOCHEMISTRY

Photochemistry explores the chemical processes that are initiated or influenced by light. It involves the study of how light, typically ultraviolet or visible light, interacts with molecules to induce chemical transformations. These reactions lead to the formation of excited states of molecules, which can then undergo various chemical processes such as bond breaking, bond formation, or isomerization.

Light excitation with a photon of suitable energy promotes a molecule from its ground state to an electronically excited state. Excitation induces alterations in the electronic structure of a molecule, changing it to be different than of the ground state. Excited states possess unique chemical and physical properties, featuring various bond distance, bond angle, geometry, redox potential and stereochemistry of the formed product.^[5]

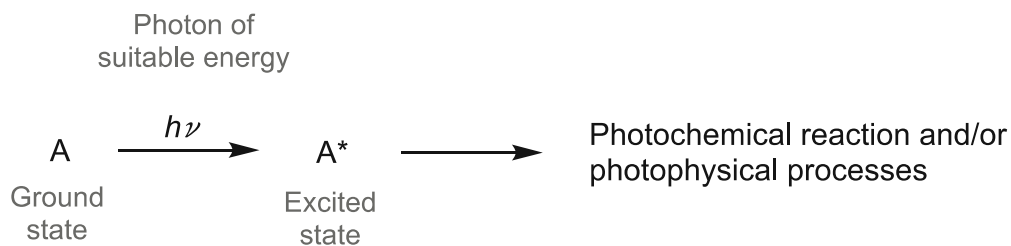


Figure 1: Excitation by light of a component A from its ground state to an electronically excited state. The excited state then undergoes deactivation by chemical reaction and/or by radiative or non-radiative photophysical processes.

The ground state takes part in traditional chemical reactions, like thermal reactions. Additionally, the ground state contributes to the absorption spectrum, determining the color of the substance.

Excited states have high energies which are thermodynamically not ideal, so there is a need to return to energetically more favorable states. This can happen as either chemical event (photochemical reactions) or involve energy loss processes, whether radiative or non-radiative. Consequently, light excitation introduces novel dimensions to both chemistry and physics.

Excited states exhibit different reactivity compared to the ground state.^[6] They are energy-rich, which means they are more reactive than the ground state. Excited state reactions usually have low or no activation energy. They have to compete with photophysical deactivation processes, so they must be very fast.

To gain a clearer understanding of the photophysical processes that are in competition, the fate of an excited state can be easily explained by to the concept of the Jablonski diagram.

1.2 JABLONSKI DIAGRAM

The Jablonski diagram serves as a visual representation of photophysical processes following irradiation. Electronic states are depicted as horizontal lines, each with its own energy level, and transitions between states are represented by arrows. Vibrational levels are shown by thin lines, with radiative and non-radiative transitions

indicated by straight and wavy arrows, respectively. The diagram illustrates events involving energy changes over time.^[5]

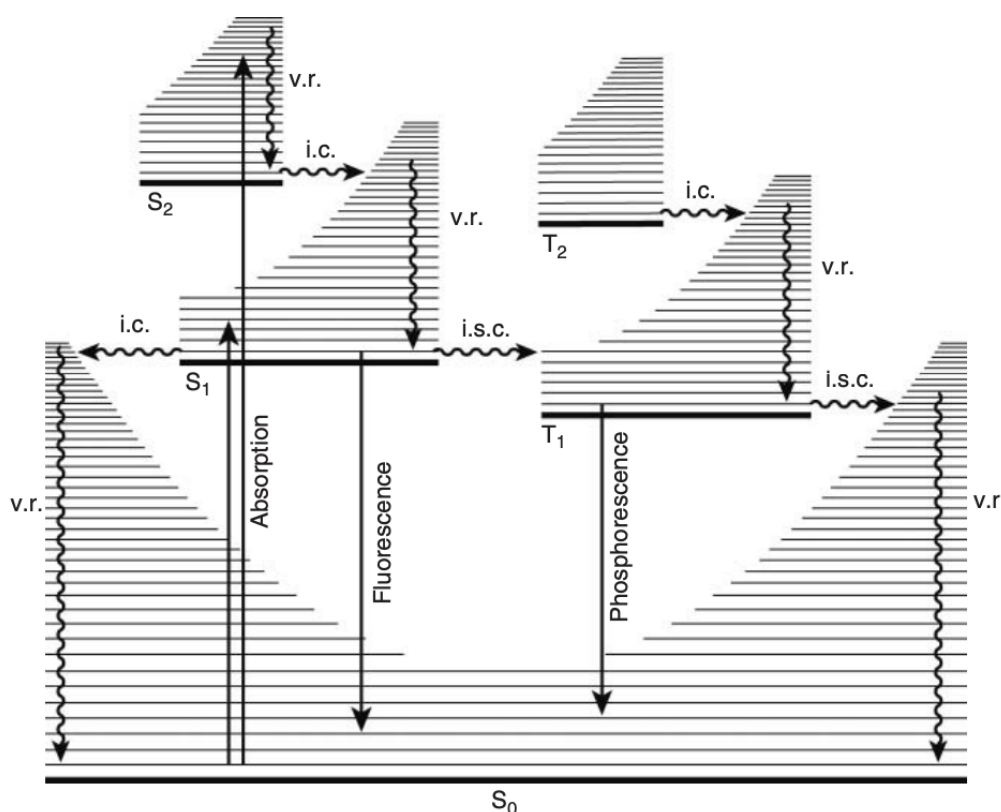


Figure 2: The Jablonski diagram. Illustration taken from the book Photochemistry and Photophysics by Balzani, Ceroni and Juris^[5]

Excitation by absorption of a photon prompts a molecule from its ground state to a higher state, to one of the singlet excited states (S_1, S_2, \dots, S_n). This process occurs rapidly, within less than 10^{-18} seconds.^[7] Subsequently, the molecule undergoes vibrational relaxation (v.r.), falling to the lowest vibrational level within the electronic state without a change in electronic energy in about 10^{-14} to 10^{-13} seconds.^[7]

Internal conversion (i.c.) follows, which results in the relaxation of the molecule into the lowest excited state of a given multiplicity manifold.

To this point all the above mentioned processes are very fast and separately not observable.^[5] The following processes are slower.

Fluorescence describes the emission of radiation during the transition from the lowest excited to the ground state. It happens without a change in multiplicity on a timescale of 10^{-9} to 10^{-8} seconds.^[7]

Several processes are competing with fluorescence. There is the possibility of a “jump” from the lowest vibrational level of the excited state to a vibrational level of about the same energy of the ground state. However, the relaxation from the first excited state to the ground state is considered the longest step, so this process is the least probable. Another possibility is the intersystem crossing (i.s.c.) to a state with a different multiplicity. This process involves a change of spin, which is forbidden, however, it can happen by spin-orbit coupling where the states can mix because of their same total angular momentum.^[8]

After the intersystem crossing (i.s.c.) from a singlet to a triplet state, relaxation to the lowest electronic state follows. From here the transition to the ground state is a slow process because the forbidden spin change must occur.

This transition can occur by the emission of photons from the T_1 state to the ground state (S_0), known as phosphorescence. Phosphorescence occurs on a much longer timescale than fluorescence (10^{-3} to 1 second and longer).^[7] In competition are the same processes as the ones with fluorescence. However, since phosphorescence is much slower, the competing processes may now compete effectively.

Due to the much longer lifetime of the excited triplet state compared to the singlet state, the photochemical reactions are more important.

1.3 THERMAL AND PHOTOCHEMICAL REACTIONS

Accurately determining the energy levels of states beyond the lowest spin-allowed and spin-forbidden excited states poses a considerable challenge due to the absence of emission and the overlapping of absorption bands. However, for the purposes of most applications, chemists are primarily concerned with the energies of the lowest excited states. Typically, an electronically excited state carries around 150 to 1250 kJ/mol more energy than its corresponding ground-state molecule.^[5] While this excess energy suggests increased reactivity in the excited state, its potential

reactivity may not translate into a chemical reaction due to the often brief lifetime of the excited state.

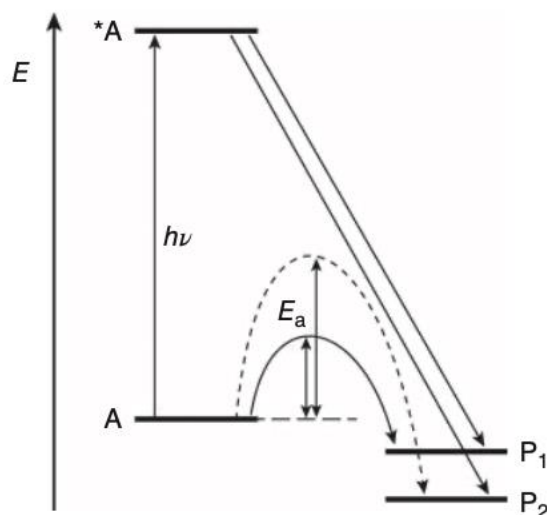


Figure 3: Schematic diagram of a reaction leading to different products that can be obtained by thermal vs. photochemical reaction. Illustration taken from the book Photochemistry and Photophysics by Balzani, Ceroni and Juris^[5]

Ground-state molecules typically follow reaction paths originating from the 'bottom' and tend to favor paths with the lowest activation energy, as illustrated by product P₁ in Figure 3. Reactions needing higher activation energies, such as those leading to product P₂ (Figure 3), may only occur under elevated temperatures or do not occur at all. During transition from the high energy states, excited states can explore reaction paths inaccessible to the ground state, resulting in the formation of products like P₂ upon photoexcitation. The diversity of available reaction paths generally increases with higher excited-state energy, contributing to the fundamental distinction between thermal and photochemical reactions.

1.4 PHOTOREDOX REACTIONS

The energy within the excited state significantly influences its electron-donating or accepting capabilities. Electronically excited molecules demonstrate enhanced electron donating and accepting abilities compared to their ground-state species.^[5]

Upon irradiation, a molecule absorbs a photon and promotes an electron to a higher energy level. The electron that has been promoted becomes more easily removable, in other words a better electron donor (reducing agent, as drawn in Figure 4) and simultaneously, a low-lying vacancy is left behind that can accept an electron (oxidizing agent, as drawn in Figure 5).^[9]

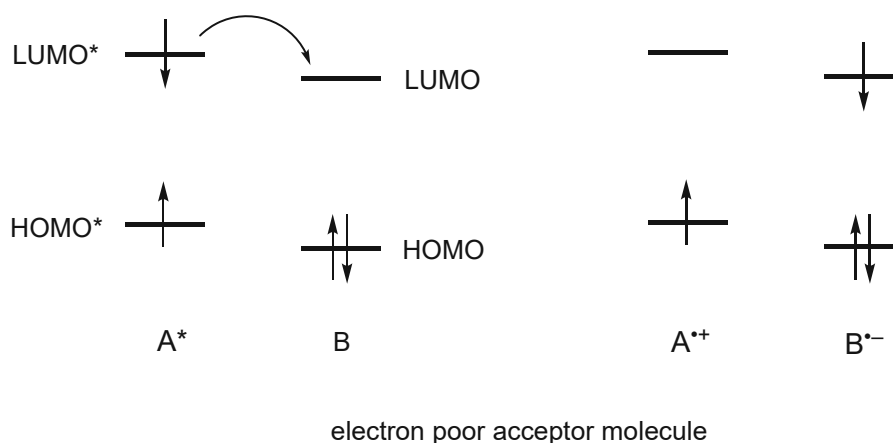


Figure 4: Molecular orbital representation of oxidative electron transfer from excited electron donor (A^*) to electron acceptor (B) (redrawn from literature^[9])

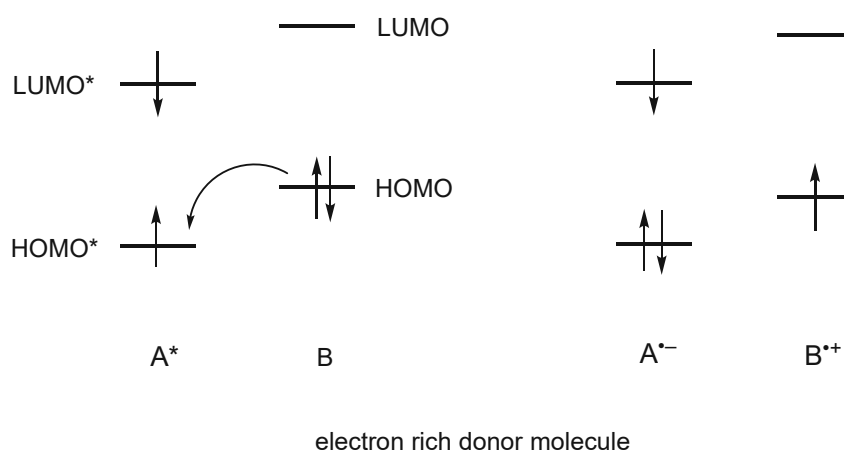


Figure 5: Molecular orbital representation of reductive electron transfer from electron donor (B) to excited electron acceptor (A^*) (redrawn from literature^[9])

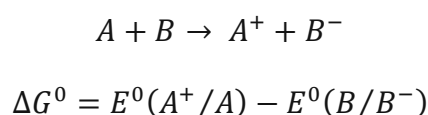
Generally, in organic molecules, the oxidation states are separated distinctly, so that an excited organic molecule can usually serve as either an electron donor or an electron acceptor, but not both.^[10] However, the photoexcited species has the remarkable property of being both more oxidizing and more reducing than the ground-state species.^[11]

This is the "peculiarity" of photochemical reactions: depending on the reactant partner, an excited molecule can function as both a reducing and an oxidizing agent, potentially performing both roles in the same (catalytic) cycle.

Photoinduced electron transfer (PET) is the primary photochemical process of the excited state. In PET, an electron is transferred between an excited-state species and a ground-state species. Figure 4 and Figure 5 show that an orbital overlap is required so that the electron transfer processes can occur by electron-exchange interactions.

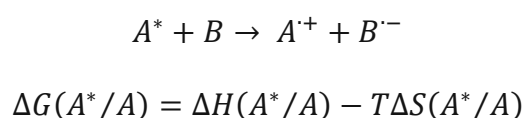
The free energy change ΔG^0 of a ground state electron transfer reaction (Eq. 1) can be calculated from the oxidation potential of the donor $E^0(A^+/A)$ and the reduction potential of the acceptor $E^0(B/B^-)$.

Equation 1: Ground state electron reaction



For a reaction involving an excited state A^* (Eq. 2), the extra amount of free energy carried by the excited state should be considered. The free energy difference between A^* and A consists of an enthalpic and an entropic term.

Equation 2: Excited state electron reaction



$\Delta H(^*A/A)$ is equal to the difference between the zero–zero vibrational levels of the excited and ground state $E_{00}(^*A/A)$ at 0 K and at room temperature if the vibrational partition functions of the two states are not very different.^[9]

The impact of entropy largely depends on contributions related to changes in dipole moment, internal degrees of freedom, and orbital and spin degeneracy. In cases where the Stokes shift is small, indicating minimal changes in shape, size, and solvation, the difference in entropy term between excited and ground states can often be neglected, allowing for reliable approximation of redox potentials using following equations.

Equation 3: Evaluation of excited state potentials after simplifications

$$E^0(A^+/A^*) = E^0(A^+/A) - E_{00}(A^*/A)$$

$$E^0(A^*/A'^-) = E^0(A/A'^-) - E_{00}(A^*/A)$$

$E_{00}(^*A/A)$ is the one-electron potential corresponding to the zero–zero spectroscopic energy of the excited state.

1.5 PHOTOCHEMICAL STRATEGIES

Visible-light-mediated chemical processes have revolutionized synthetic chemistry by providing precise control over radical generation and excited-state transformations.^[12] The key mechanism involves the generation of radical species through single electron transfer (SET) between the substrate and a photoexcitable molecule.

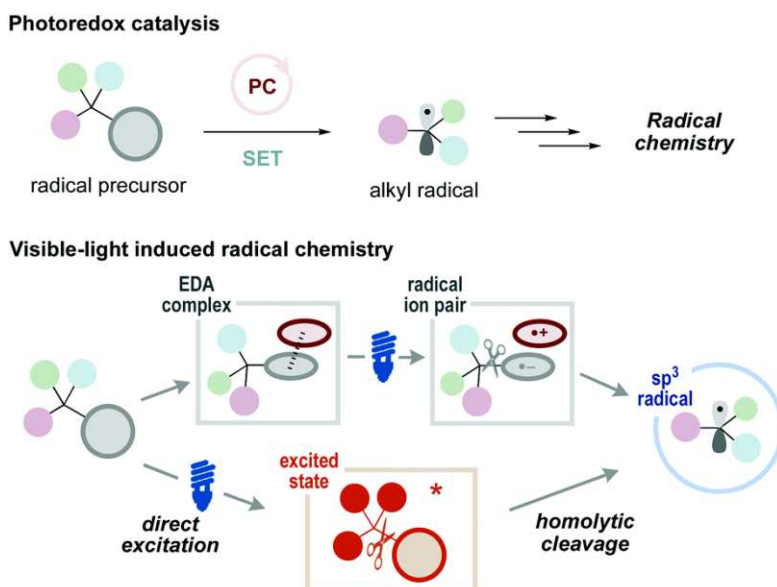


Figure 6: Types of photochemical reactions. Figure taken from ^[12]

In a photoredox catalytic reaction, small quantities of a catalyst are utilized, capable of inducing chemical transformations in reaction partners upon absorption of light. The photocatalyst's excited state interacts iteratively with the reaction partners, leading to the formation of reaction intermediates. Subsequently, the photocatalyst regenerates itself in each cycle of these interactions.

The direct excitation strategy eliminates the need for a photoredox catalyst. Direct photoexcitation refers to a process in which a molecule absorbs light energy directly, leading to an excited state. This absorbed energy can induce bond cleavage, generating radicals and initiating chemical reactions.

The formation of an electron-donor-acceptor (EDA) complex involves the dipole-dipole interactions between an electron donor and an electron acceptor to form a reversible, weak ground-state aggregate. This complexation can influence the electronic structure of the molecules involved and impact their reactivity. Generally,

upon light irradiation, the EDA complex turns into the excited state, causing an electron transfer to give radicals and to initiate subsequent reactions.

1.5.1 PHOTOREDOX CATALYSIS

The fundamental concept of photoredox chemistry involves the excitation of a photoredox catalyst under visible light irradiation, initiating a single electron transfer (SET) to either an acceptor or a donor. This SET event leads to the catalyst either losing an electron (in an oxidative quenching cycle) or gaining an electron from the substrate (in a reductive quenching cycle). The catalyst subsequently undergoes the reverse process, engaging in a SET with another substrate, often the original one, thereby completing the catalytic cycle (Figure 7).

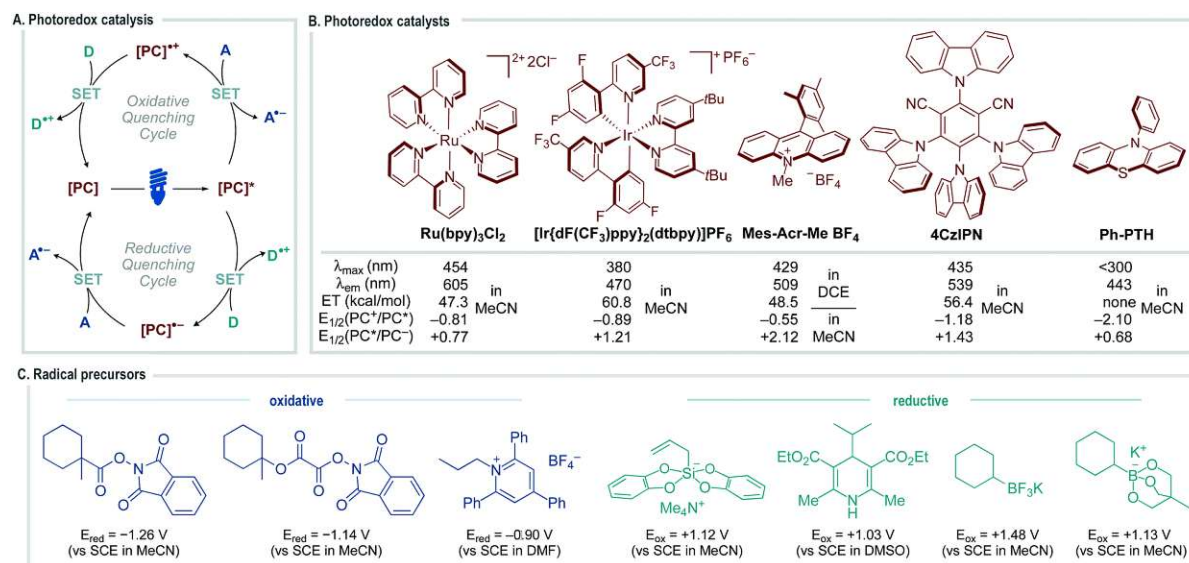


Figure 7: (A) General catalytic mechanism of photoredox catalysis. (B) Widely used photoredox catalysts and their photophysical properties. Figure taken from ^[12]

Iridium and ruthenium complexes are the most widely used metal photocatalysts. ^[12] Recently, there has been significant progress in the development of organophotoredox catalysts. ^[13] The design and synthesis of innovative organophotoredox catalysts have advanced alongside the utilization of well-established organic fluorescent dyes as photoredox catalysts.

The production of radicals depends on the redox potential of individual radical precursors, allowing for either oxidative or reductive quenching. Chemists have the flexibility to design the desired catalytic reaction by considering the inherent redox potential of both the photoredox catalyst and the radical precursor.

1.5.2 DIRECT PHOTOEXCITATION OF REACTION SUBSTRATES

The most straightforward method for radical generation is the direct photoexcitation of reaction substrates, wherein the radical precursor itself absorbs visible light, and the acquired energy is utilized for bond cleavage, leading to radical generation.

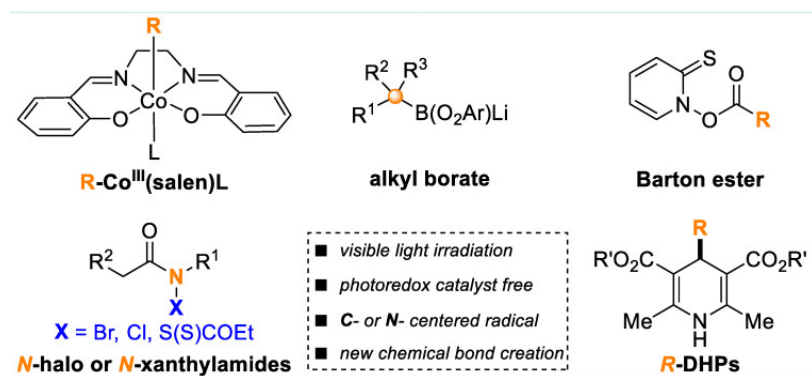


Figure 8: Commonly used molecules for direct photoexcitation. Figure taken from ^[14]

Structural analogues of vitamin B12, Barton ester and alkyl borates can function as radical sources, facilitating the creation of new C-C bonds through direct photoexcitation under visible light irradiation.^[14] A wide range of N-halo and N-xanthylamides, which, under photoirradiation, undergo homolytic cleavage of the N-X bond to generate amidyl radicals were also developed.^[15, 16] More recently, the Melchiorre group discovered that the direct photoexcitation of 4-R-1,4-dihydropyridines (R-DHPs) leads to the formation of an R radical.^[17] This radical is then effectively employed in cross-coupling reactions using a Nickel complex as an electron mediator (Figure 9).

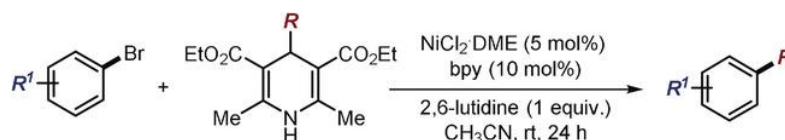


Figure 9: Nickel-catalysed cross-coupling process enabled by the photochemical activity of the 4-R-1,4-dihydropyridine. Reaction mixture was irradiated with LED $\lambda=405$ nm^[17]

1.5.3 EDA COMPLEX FORMATION

According to Mulliken's charge-transfer theory, the interaction between an electron-rich substrate (donor) and an electron-poor molecule (acceptor) can lead to the formation of an EDA complex in the ground state.^[18] The physical properties of an EDA complex differ from the individual substrates due to the creation of new molecular orbitals resulting from the electronic coupling of D and A orbitals (HOMO/LUMO). This new chemical entity is characterized by the emergence of a distinct absorption band known as the charge-transfer band.^[19]

Melchiorre and colleagues used the EDA complex strategy within the framework of asymmetric organocatalysis, facilitating the α -alkylation of aldehydes.^[20] They created a colored EDA complex by combining an electron-deficient benzyl bromide with a chiral enamine formed in situ from aldehyde using an amine catalyst (Figure 10). This chiral EDA complex, when exposed to visible-light irradiation, undergoes single electron transfer (SET) to generate a radical ion pair. The elimination of the leaving group, the bromide anion, from the acceptor results in the alkyl radical, ultimately leading to radical-radical coupling and the formation of the product.

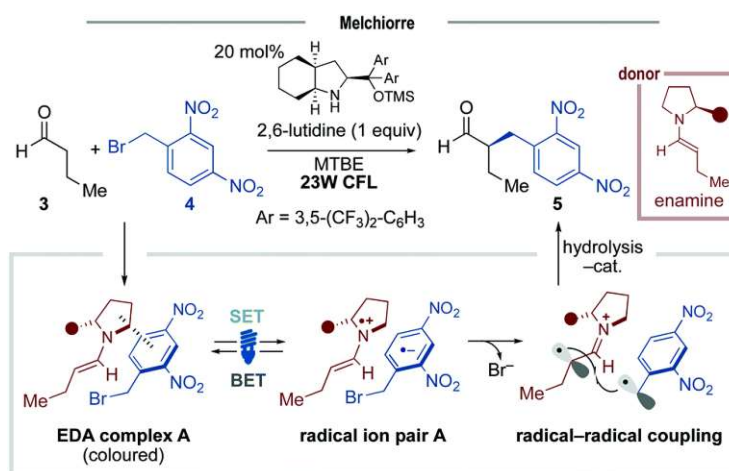


Figure 10: Enantioselective catalytic α -alkylation of aldehydes. Figure taken from^[12]

1.6 HANTZSCH ESTERS

The synthesis of Hantzsch esters (1,4-dihydropyridine dicarboxylates) was first reported in 1881 by Arthur Rudolf Hantzsch.^[21] With the introduction of organocatalytic transfer hydrogenations in the early 2000s, Hantzsch esters (HEs) have been found to be useful for various applications across organic chemistry.

One reason for the importance of HEs is that they are chemically similar to 1,4-dihydronicotinamide, which is a part of the NADH coenzyme. NADH and NADPH are common electron donors in bio-redox reactions, but are expensive and unstable.^[22] In contrast, NAD(P)⁺ is a more stable and affordable oxidized form, serving as a native electron acceptor. NAD(P)H structurally contains the 1,4-dihydronicotinamide moiety. They can either bind to the enzyme scaffold and be regenerated *in situ* or be recycled in a non-binding manner, often requiring supplementation or artificial regenerating systems.^[23] HEs, with a 1,4-dihydropyridine moiety similar to NAD(P)H, are economical and stable electron donors widely used in abiotic organic synthesis.^[24]

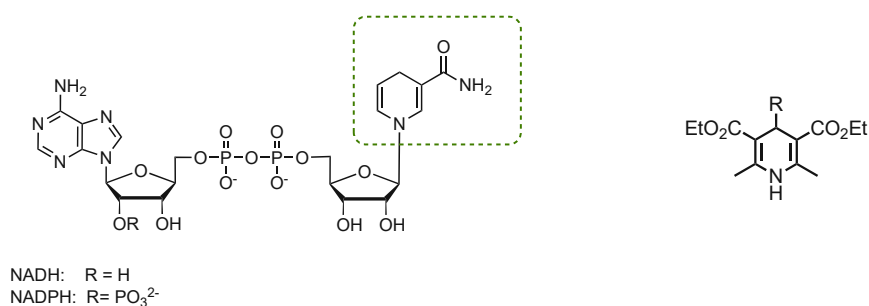


Figure 11: Nicotine amide of NAD(P)H marked in green square and a Hantzsch ester on the right

HEs have also proven to be very important hydrogen sources in catalytic hydrogenation reactions through asymmetric transfer hydrogenation processes.^[25] Asymmetric catalysis is a key focus in modern synthetic chemistry, enabling the efficient synthesis of enantiopure compounds using just small amounts of chiral molecules. Asymmetric hydrogenation was recognized with a Nobel Prize in Chemistry in 2001. Traditional processes use hydrogen gas as the reducing agent with transition metal-based chiral catalysts^[26, 27], while the analogous transfer hydrogenation employs other hydrogen sources, like isopropanol and formic acid.^[28, 29]

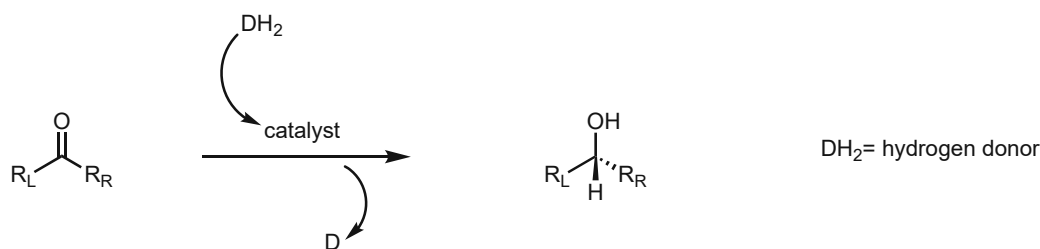


Figure 12: Schematic illustration of transfer hydrogenation reactions

Despite high reactivity and selectivity, challenges include limited substrate scope and difficulties in catalyst separation and recycling.^[25] Inspired by nature's efficient asymmetric transfer hydrogenations (ATH) using enzymes and organic cofactors, chemists have also developed biomimetic, metal-free ATH approaches. Hantzsch ester and other heterocyclic compounds can effectively mimic NADH in such processes, and serve as hydrogen donor, leading to successful reduction of double bonds (C=C, C=N, and C=O) under mild conditions, providing versatile chiral building blocks and practical syntheses of complex molecules and natural products.^[25]

The molecular transformation of unstrained carbon–carbon (C–C) bonds poses a significant challenge in organic chemistry^[30, 31], particularly in developing C–C bond-forming reactions between fragments generated from C–C bond-cleavage reactions of independent substrates.^[32] This difficulty led to the exploration of photoredox catalysis for C–C bond activation and transformation, as radical cations and radical anions formed during single-electron-transfer processes are considered suitable intermediates.^[11, 33, 34]

A promising approach involves generating radical cations through the single-electron oxidation of amines to achieve rapid C–C bond-cleavage reactions.^[35-38] Several research groups have successfully conducted oxidative C–C bond-cleavage reactions of amines using photoredox catalysts.^[39-41]

In addition to these reactions, aromatic substitution reactions of cyanoarenes with various alkylating reagents under UV and visible light have garnered interest.^[42, 43] These reactions proceed through radical–radical coupling reactions between a cyanoarene radical anion and an alkyl radical, followed by C–C bond-cleavage of the resulting alkylated cyanoarene.

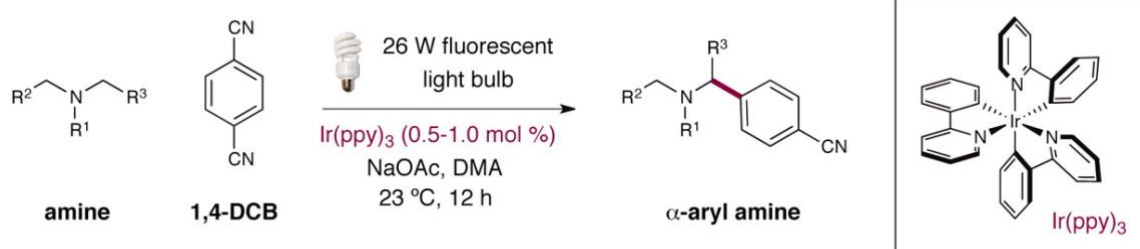


Figure 13: Photoredox C-H-arylation of amines. Graph taken from [43]

A novel approach was designed by Nishibayashi, Nakajima and Sakata for photoredox-catalyzed aromatic substitution reactions of cyanoarenes with alkylating reagents.^[32] This involved generating alkyl radicals from C–C bond-cleavage reactions of alkylating reagents, specifically using cyclic amines like 4-alkyl-1,4-dihydropyridines. The study revealed successful aromatic substitution reactions, achieving C–C bond-forming reactions between fragments generated from C–C bond-cleavage reactions of independent substrates, a unique reaction not previously demonstrated with visible light-photoredox catalysis.

Recently, there were examples published for carbamoyl radical transfer from HE to activated olefins and imines using metal free organocatalysts^[44, 45] and also for acyl radical transfer onto electron-poor alkenes under visible light without the use of any catalyst or additive^[46].

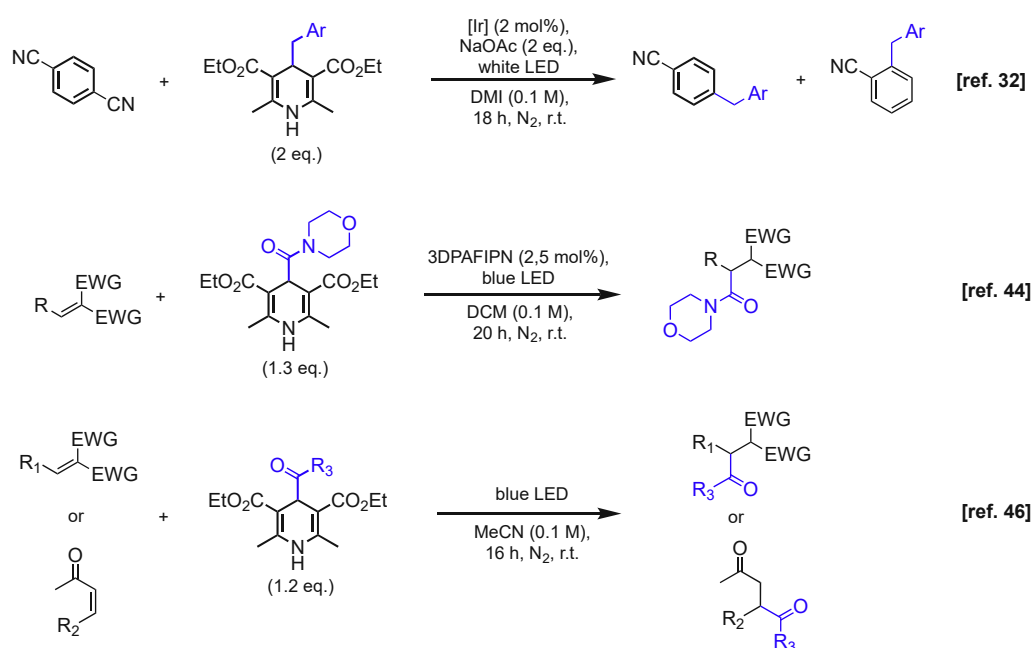


Figure 14: Examples from the literature using Hantzsch esters for C-C bond forming reactions^[32, 44, 46]

2 AIM OF THE THESIS

Under (visible) light-irradiation, Hantzsch esters can serve as powerful radical reservoirs. As such, they were proven to be invaluable reagents for transferring alkyl-, acyl-, aryl- and carbamoyl moieties under photocatalytic or catalyst-free conditions (Figure 15).^[47]

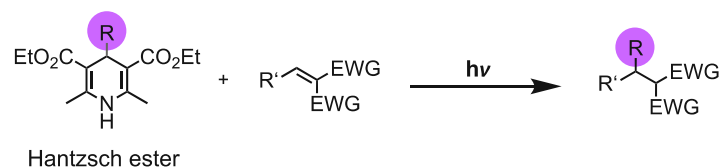


Figure 15: General scheme of the radical transfer reaction

Being inspired by the limitations of such processes, the aim of this work was to use the HE as an acetal radical reservoir and to transfer the acetal group from the HE to electron poor olefine substrates. This can be achieved by directly exciting the HE by light. This leads to the cleavage of the acetal radical which then reacts with the activated substrate. After acetalization, these products can be used as precursors for the synthesis of formylated final products (Figure 16).

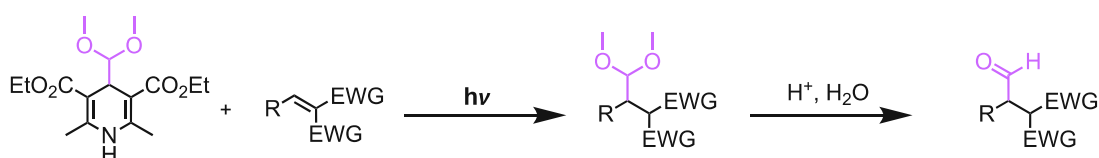


Figure 16: Acetalization of olefine substrate and synthesis of aldehyde

While the use of formylated HEs might seem a reasonable idea, the photochemical irradiation of such Hantzsch ester does not lead to the formation of formylated products. The reason for this is that the generated formyl radical is too unstable so it cannot be transferred directly; however, the acetal and thianyl radicals are stable enough to undergo the controlled radical reaction; underlining the necessity for acetal or thioacetal moieties for such transformations (Figure 17).

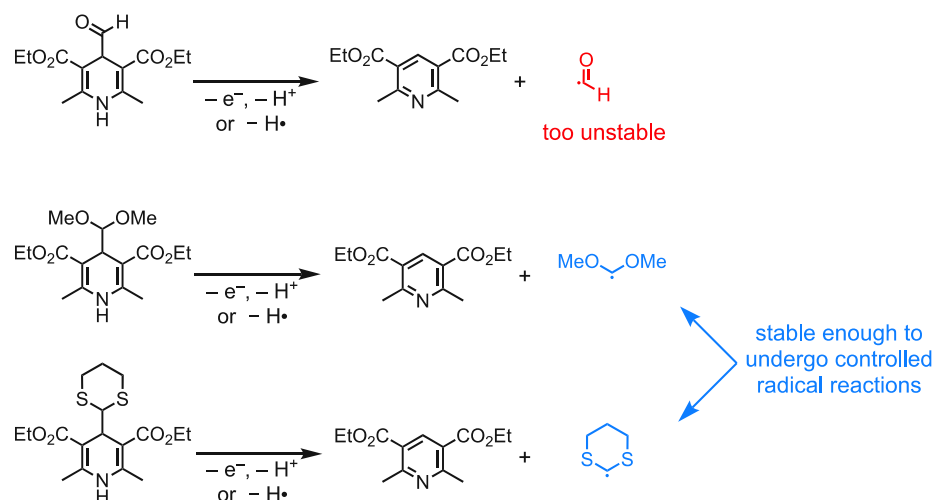


Figure 17: The formation of acetal radicals *via* photoexcitation of Hantzsch esters

In the literature, there are a few reports that used 4-dimethoxymethyl HE as part of the substrate scope (Figure 18).^[48-50]

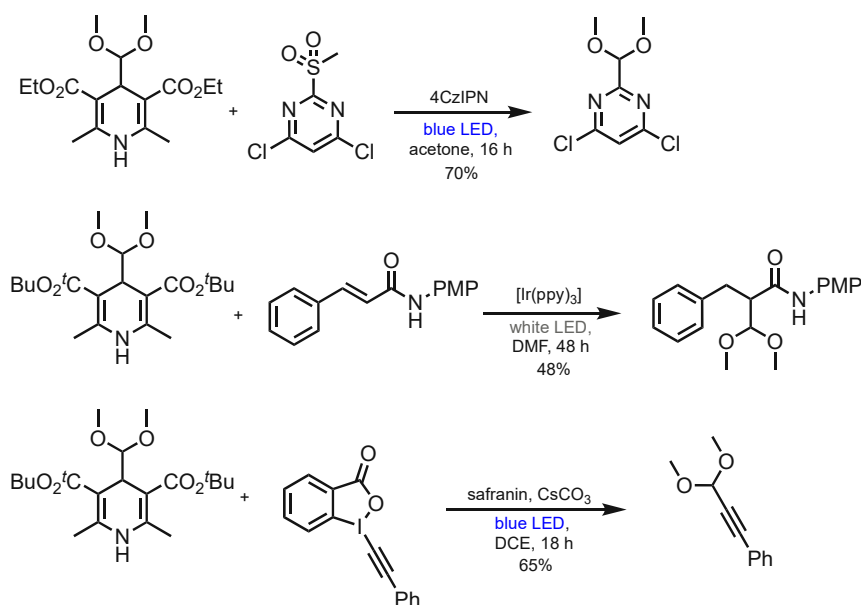


Figure 18: Examples for photochemical transformation using 4-dimethoxymethyl HE reagents^[48-50]

Nevertheless, all three approaches use photocatalysts for these reactions; furthermore, 4-dithianyl substituted HE are not yet mentioned in the literature. This encouraged us to investigate the applicability of 4-substituted Hantzsch esters featuring either acetal or a thioacetal moieties as radical reservoirs as a potential

novel approach for the formylation of various electron-poor acceptors. Aiming for an optimized method which works under mild reaction conditions – room temperature, atmospheric pressure – we envisioned the application of this method for a wide range of different substrates.

3 RESULTS AND DISCUSSION

3.1 HANTZSCH ESTER SYNTHESIS

A very broad variety of Hantzsch ester derivatives can be prepared by the Hantzsch ester synthesis.^[21] The 4-dimethoxymethyl-Hantzsch ester (**HE 1**) was also prepared by the classical Hantzsch ester synthesis.

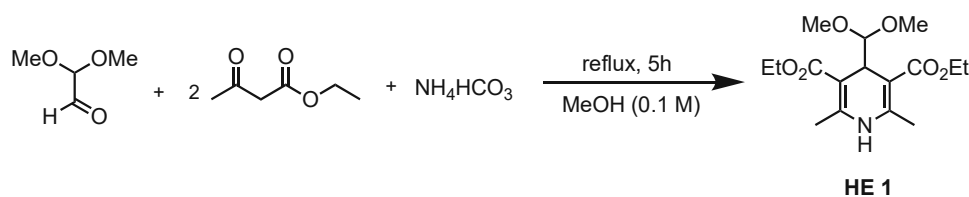
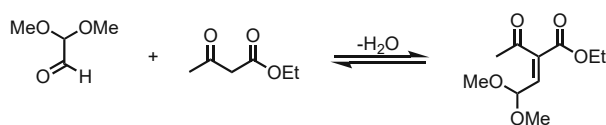


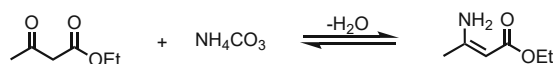
Figure 19: Hantzsch ester synthesis

The reaction proceeds through the Knoevenagel condensation of the aldehyde and one equivalent of the ethyl acetoacetate to form the first key intermediate. In a parallel reaction an ester enamine is formed as the second intermediate from the other one equivalent of ethyl acetoacetate and ammonium bicarbonate, as nitrogen source. Further condensation of these two fragments gives the dihydropyridine derivative. The mechanism of the reaction is shown in Figure 20.

Knoevenagel condensation:



Enamine formation:



Condensation of the two fragments:

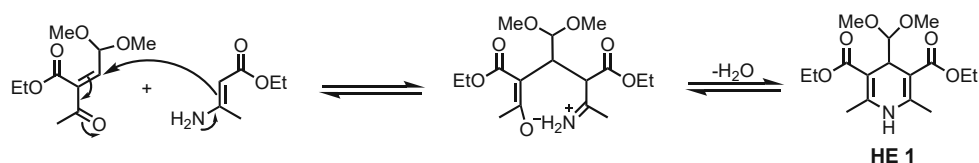


Figure 20: Mechanism of Hantzsch ester synthesis

The preparation of the 4-(1,3-dithianyl)-Hantzsch ester (**HE 2**) failed *via* classical Hantzsch ester synthesis. Instead of providing the desired Knoevenagel condensate (**P 2**) as the first key intermediate, the isomeric ketene thioacetal (**P 3**) was isolated.

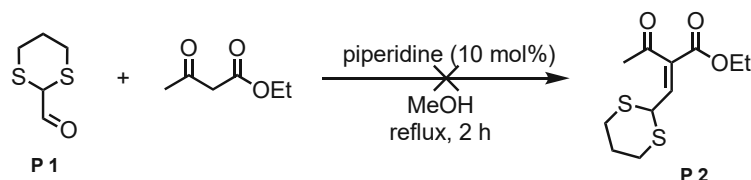


Figure 21: The desired condensation product

The condensation product probably did form and the isolated product is possibly the result of an isomerization by the base (piperidine) present in the reaction medium. Meyers and Strickland suggests that the ketene thioacetal product is thermodynamically more favourable, because there is substantial ring strain relief when the 2 position of the 1,3-dithiane ring is sp^2 hybridized.^[51] Additionally, the overlap of the 3p-orbitals of the two adjacent sulphur atoms with the 2p-orbital of the carbon atom is enhanced, which has a stabilizing effect on the structure.

Following the isomerization, the acyl group was likely cleaved by piperidine through a “reverse” aldol reaction. After protonation the ketene thioacetal (**P 3**) was formed. The possible reaction mechanism is shown in Figure 22.

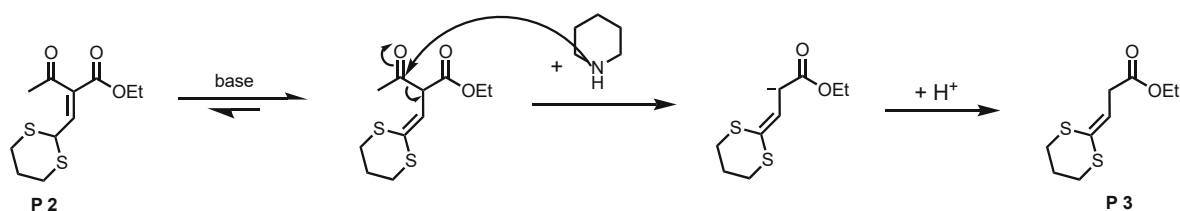


Figure 22: Possible reaction mechanism of the ketene thioacetal formation

Because of the above-mentioned reasons, the conventional Hantzsch ester synthesis proved to be unemployable to prepare the dithianyl Hantzsch ester (**HE 2**). However, given that the 4-dimethoxymethyl Hantzsch ester (**HE 1**) can be easily synthesized in a multi-gram scale, it was used as the initial substrate for the synthesis of the

dithianyl Hantzsch ester, in which the dimethoxymethyl moiety was replaced by the dithianyl group.

Two methods were employed to prepare the dithianes from the acetal and 1,3-propanedithiol, employing boron trifluoride diethyl etherate as an Lewis acid catalyst according to literature procedure.^[52] The first procedure included the formation of a silyl modified reagent (**P 4**).

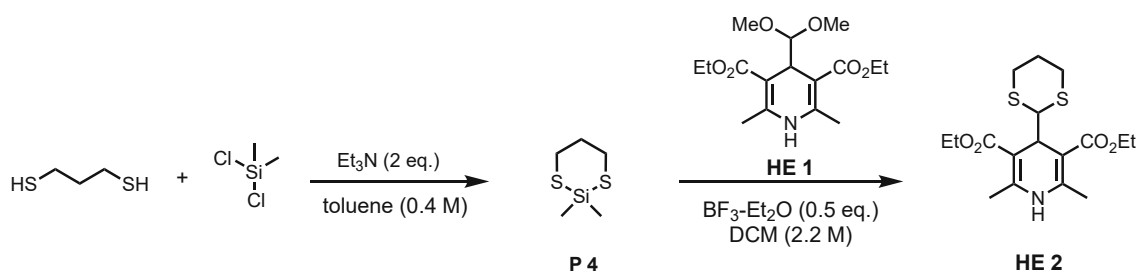


Figure 23: Dithianyl group introduction through silyl modification^[52]

This protocol is especially useful if there are ketones and aldehydes competing in the same reaction, because the silyl reagent is completely selective for the aldehydes.^[52] Since in the case of the formation of the desired HE there are no competing ketones, 1,3-propanedithiol was used directly. This reaction resulted in the desired product with good yield (74%), prompting its utilization for scale-up due to fewer steps compared to the above-mentioned method.

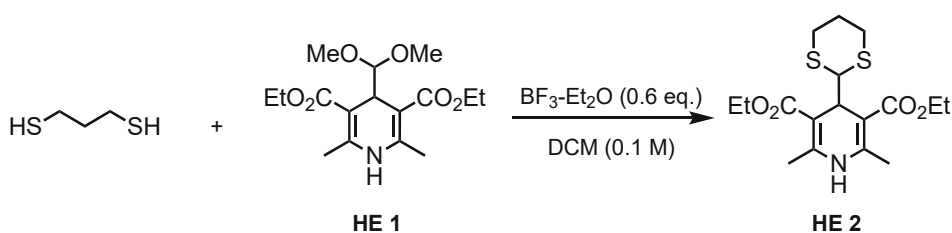


Figure 24: Dithianyl group introduction using 1,3-propane dithiol

3.2 PHOTOREACTION DESIGN

3.2.1 INVESTIGATIONS OF THE UV-VIS ABSORPTION PROPERTIES

3.2.1.1 UV-VIS ABSORPTION OF THE HANTZSCH ESTER (**HE 2**)

The determination of the absorbance properties of the substrates is the starting point of any photochemical methodology development.

In the pursuit of defining the optimal wavelength and selecting the most appropriate light source for the reactions, an analysis of the absorbance spectrum of the Hantzsch ester (**HE 2**) was conducted using UV-VIS spectroscopy. The colourless appearance of **HE 2** already indicated a lack of extensive conjugation, and therefore its lack of absorbance in the visible light region. For the UV-VIS measurement, a 0.3 mM solution of **HE 2** in acetonitrile was prepared and measured. The resulting spectrum is shown in Figure 25. The maximum absorption is at a wavelength of 325 nm.

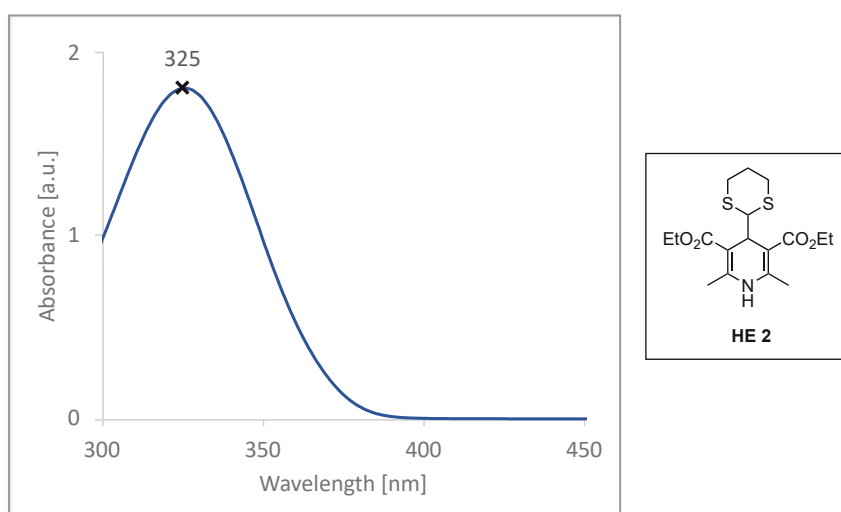


Figure 25: UV-VIS absorbance spectrum of **HE 2**

3.2.1.2 UV-VIS ABSORPTION OF THE REACTION MIXTURE

Optical absorption spectroscopic studies of the reaction mixture are important to conduct, to detect if a visible light-absorbing electron-donor-acceptor (EDA) complex is formed between the Hantzsch ester and the substrate and whether this complex is the one undergoing excitation.

To investigate the potential formation of an EDA complex between the model substrate, benzylidene malononitrile (**S 1**) and the Hantzsch ester (**HE 2**), the absorbance of both components at the same concentration (3 mM in MeCN) were individually measured by UV-VIS spectroscopy. Additionally, a 1:1 mixture of the two components in the same concentration was also measured.

If an EDA complex is formed, the absorbance of the complex – the substrate-reagent mixture – would differ from the absorbance of the individual components. The results indicate that the absorbance of **HE 2** and the mixture are overlapping with each other and basically identical, as depicted in Figure 26. Consequently, it can be inferred that HE is directly excited by the irradiation and no EDA complex formation occurs in this process.

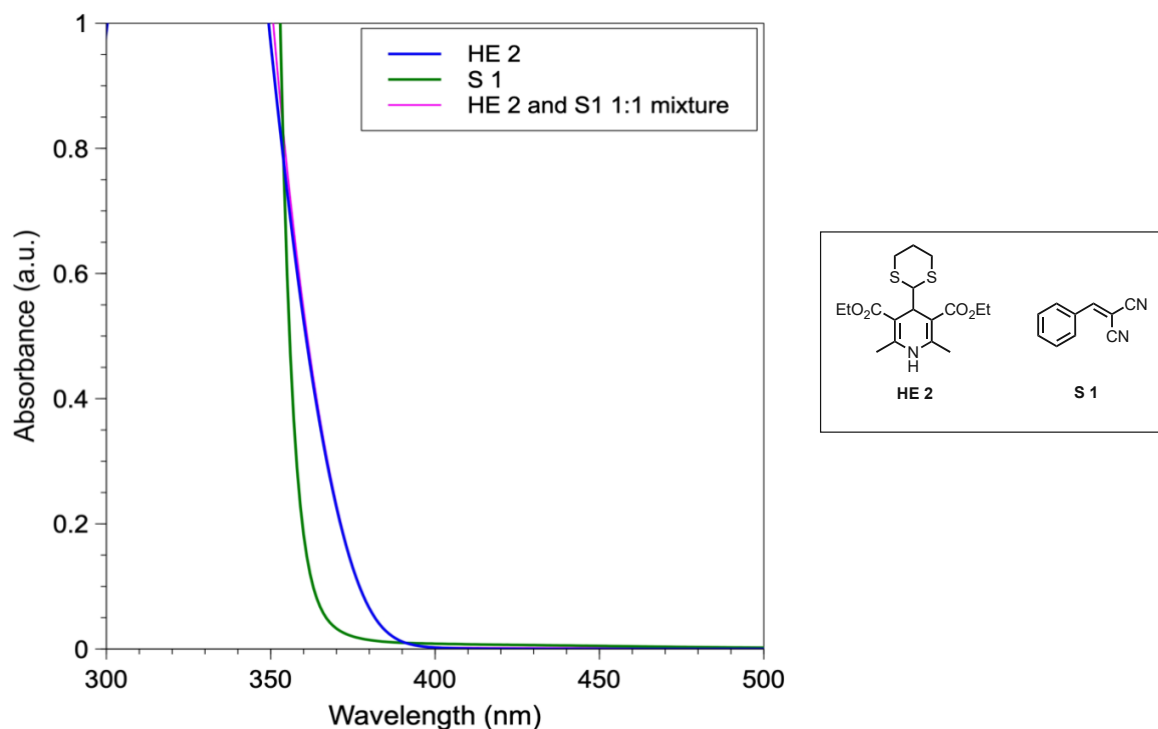


Figure 26: UV-VIS absorption spectra of **HE 2** (blue), **S 1** (green) and a 1:1 mixture of **HE 2** and **S 1** (pink)

3.2.2 OPTIMIZATION OF THE REACTION CONDITIONS

With the initial analysis in hand, the reaction parameters were optimized for the hydrodithioacetalization of benzylidene malononitrile. After the analysis of the absorption profile of the reaction components, a light source with a wavelength of 365 nm was chosen. At this wavelength the absorption of **HE 2** is strong enough, but the absorption of the model substrate, benzylidene malononitrile (**S 1**) is minimized to avoid undesired reactivity (as shown earlier on Figure 26).

In light of extensive literature concerning reactions involving Hantzsch esters, the majority of these studies employed either acetone or acetonitrile for the reactions.^[46, 53] Consequently, for the purpose of optimizing this reaction, these two solvents were tested. Both worked quite well, resulting in high yields of the product (entries 1 and 5). Acetonitrile performed slightly better, so it was chosen for the optimization of the other parameters.

The reaction time was optimized subsequently. After 6 hours the yield was already good, but it was improved to 88% by increasing the reaction time to 16 hours (entries 2-3).

Table 1: Reaction optimization under near UV light

Entry ^a	Solvent	Wavelength (nm)	Reaction time (h)	Yield (%) ^b
1	Acetonitrile	365	16	88
2	Acetonitrile	365	6	72
3	Acetonitrile	365	4	54
4	Acetonitrile	365	2	23
5	Acetone	365	16	85

^a Performed with 0.1 mmol benzylidene malononitrile (**S 1**), 0.12 mmol Hantzsch ester (**HE 2**) in 1 mL solvent at room temperature under N₂ atmosphere. ^b Yields determined *via* ¹H NMR using 1,3,5-trimethoxybenzene as internal standard.

To enable the reactions under visible light irradiation, we aimed to evaluate the compatibility of our reaction system with a photocatalyst. Following the principles of green chemistry, we opted for organo-based photocatalysts instead of the more conventional precious metal-based ones.

Subsequently, we conducted tests on two cyano-arene-based photocatalysts, 2,4,6-tris(diphenylamino)-3,5-difluorobenzonitrile (3DPA2FBN) and on 1,2,3,5-tetrakis(carbazole-9-yl)-4,6-dicyanobenzene (4CzIPN), as well as Na₂-Eosin Y, a xanthene-based photocatalyst. The photocatalysts are shown in Figure 27; meanwhile, their reactivity is depicted in Table 2.

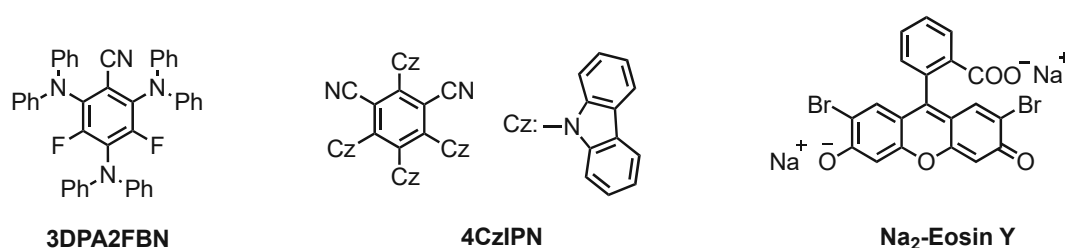


Figure 27: Organo-photocatalysts tested for the reaction

Table 2: Optimization of the reaction conditions with a photocatalyst

Entry ^a	Photocatalyst	Wavelength (nm)	Yield (%)
1	3DPA2FBN	450	81
2	4CzIPN	450	89
3	Na ₂ -Eosin Y	525	79

^a Performed with 0.1 mmol benzylidene malononitrile (**S 1**), 0.12 mmol Hantzsch ester (**HE 2**) and 2.5 mol% photocatalyst in 1 mL solvent at room temperature under N₂ atmosphere. ^b Yields determined via ¹H NMR using 1,3,5-trimethoxybenzene as internal standard.

Each of the three catalysts performed well; however, 4CzIPN (entry 2) proved to be the most efficient. Consequently, we selected this particular photocatalyst to further investigate the substrate scope under visible light irradiation.

3.2.3 REACTION SETUP

Synthetic photoredox chemistry has evolved into a versatile tool; however, numerous publications do not utilize commercial reactors and the conditions for reaction setups lack a standardized framework.^[54] There is considerable variability in laboratory preferences, prompting the need to assess different systems. To achieve precise temperature control, options such as water and fan cooling were available. For illumination, commercially available 15 W and 30 W LED lamps acquired from Hepatochem were employed.

All photoreactions were conducted in an EvoluChem™ PhotoRedOx reactor, which incorporates mirrors internally to maximize the exposure of the reaction mixture to the photon stream.

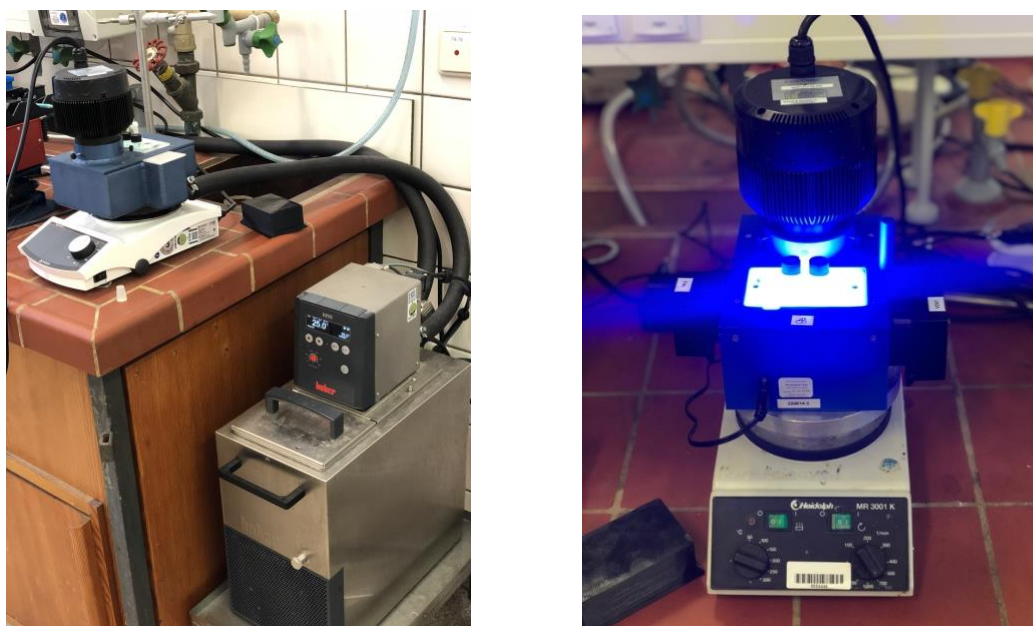


Figure 28: Pictures of the reactor setup with water cooling (on the left) with fan cooling (on the right)

The evaluation of the effect of the different light sources and temperature control was done on the model reaction shown in Table 3.

Table 3: Evaluation of the LED light sources ($\lambda=365$ nm)

Entry	Rel. irradiance	Yield (%) ^b
1	9 mW/cm ² (15 W)	86
2	15 mW/cm ² (30 W)	88

Performed with 0.1 mmol benzylidene malononitrile (**S 1**), 0.12 mmol Hantzsch ester (**HE 2**) in 1 mL solvent at 25 °C (water bath) and $\lambda=365$ nm under inert gas atmosphere. ^a Yields determined via ¹H NMR using 1,3,5-trimethoxybenzene as internal standard.

There was no significant difference in the yields observed (Table 3).

The temperature was regulated through either fan cooling, fluctuated between 30-35 °C (measured on the outside of the glass vial), or through water cooling (25 °C water bath). No difference between the yields was observed (Table 4).

Table 4: Evaluation of the temperature control

Entry	Temperature control	Yield (%) ^b
1	Fan cooling	88
2	Water bath	88

Performed with 0.1 mmol benzylidene malononitrile (**S 1**), 0.12 mmol Hantzsch ester (**HE 2**) in 1 mL solvent at $\lambda=365$ nm (15 mW/cm²) under inert gas atmosphere. ^a Yields determined via ¹H NMR using 1,3,5-trimethoxybenzene as internal standard.

Choosing the LED lamp with the stronger relative irradiance and the water bath as temperature control, the reproducibility of the reaction was tested. The results are shown in Table 5.

Table 5: Evaluation of the reproducibility of the model reaction

Entry	Yield (%) ^b
1	88
2	88
3	85

Performed with 0.1 mmol benzylidene malononitrile (**S 1**), 0.12 mmol Hantzsch ester (**HE 2**) in 1 mL solvent at $\lambda=365$ nm (15 mW/cm²), at 25 °C (water bath) under N₂ atmosphere. ^a Yields determined *via* ¹H-NMR using 1,3,5-trimethoxybenzene as internal standard

With the same reaction setup, the reproducibility of the reaction with 4CzIPN as a photocatalyst was also tested (

Table 6). For this reaction, a LED lamp at $\lambda=450$ nm and a relative irradiance of 55 mW/cm² was used.

Table 6: Evaluation of the reproducibility of the model reaction with 4CzIPN as a photocatalyst

<p> <chem>C#N/C=C/c1ccccc1</chem> (1.0 eq. S 1) + <chem>CCOC(=O)C1=C(C)NC(=C1C(=O)OCC)C2SCCSC2</chem> (1.2 eq. HE 2) $\xrightarrow[\text{MeCN (0.1 M), 16 h, N}_2]{\text{4CzIPN (2.5 mol\%), 450 nm}}$ <chem>C#NCCc1ccccc1</chem> (1b) </p>	
Entry	Yield (%) ^b
1	89
2	89
3	83

Performed with 0.1 mmol benzylidene malononitrile (**S 1**), 0.12 mmol Hantzsch ester (**HE 2**), 2.5 mol% of 4CzIPN in 1 mL solvent at $\lambda=450$ nm (55 mW/cm²), 25 °C (water bath) under inert gas atmosphere. ^a Yields determined via ¹H-NMR using 1,3,5-trimethoxybenzene as internal standard

Both model reactions were reproducible.

3.3 REACTION DEVELOPMENT

3.3.1 SUBSTRATE SCOPE

After identification of the ideal reaction conditions, the transfer acetalization of electron poor olefins was further investigated with different substrates to determine the scope and limitation of the system. Hantzsch esters **HE 1** and **HE 2** were both employed to explore the substrate scope.

The yields of the products that were formed using **HE 1** are represented in columns 3 and 4 of Table 7, the former without and latter with the use of photocatalyst (4CzIPN). The yields of the products that were formed with **HE 2** with Eosin Y as the photocatalyst are shown in column 5 of Table 7. As such, a total of 63 reactions were investigated.

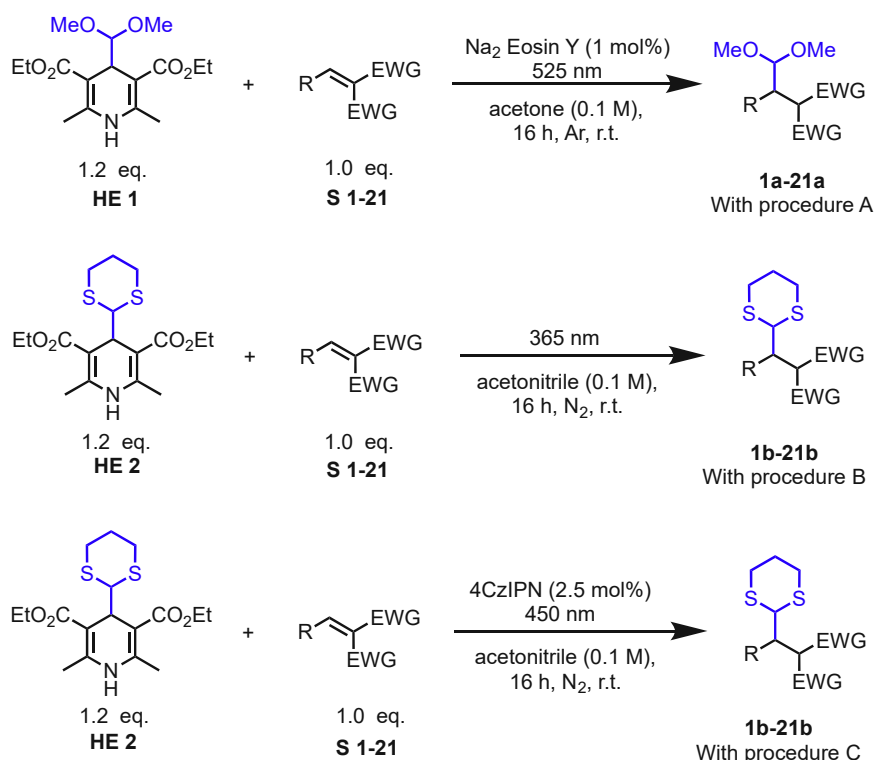
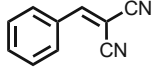
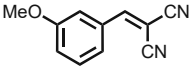
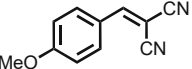
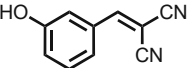
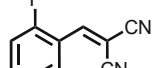
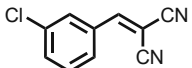
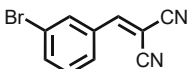
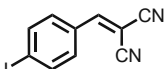
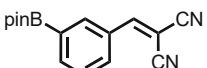


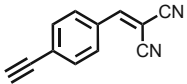
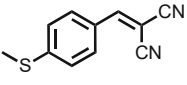
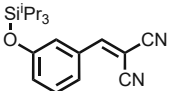
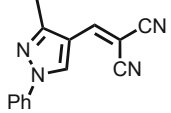
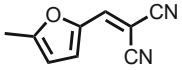
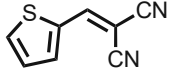
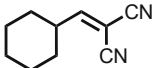
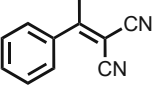
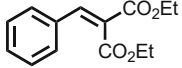
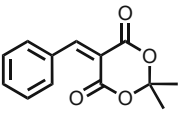
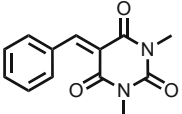
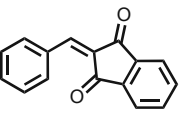
Figure 29: Procedures for the exploration of the substrate scope for the transfer (thio)acetalization

The primary focus of the substrate scope centred on the dicyanide compounds, although other electron withdrawing groups such as esters, imides and ketones were tested as well (entries 18-21). In the case of the non-cyclic ester (entry 18) the

reaction with the dithianyl HE (**HE 2**) proved unsuccessful due to steric hindrance of the dithianyl-group (**18b**). This conclusion is sustained by the successful reaction of HE with the considerably smaller acetal group (**HE 1**), resulting in good yield (**18a**). Steric hindrance also posed a challenge with a substrate featuring a tertiary target centre (entry 17). While the formation of **17b** was not observed with **HE 2**, **17a** demonstrated a satisfactory yield, probably because the acetal group is smaller in case of **HE 1**.

Table 7: Substrate scope

Entry	Substrate	Product and Yield Proc. A ^a	Product and Yield Proc. B ^b	Product and Yield Proc. C ^c
1	 S 1	1a (84%) ^e	1b (86%) ^e	1b (89%) ^d
2	 S 2	2a (86%) ^e	2b (85%) ^d	2b (88%) ^d
3	 S 3	3a (80%) ^e	3b (70%) ^d	3b (67%) ^d
4	 S 4	4a (67%) ^e	4b (96%) ^d	4b (93%) ^d
5	 S 5	5a (60%) ^e	5b (72%) ^d	5b (91%) ^d
6	 S 6	6a (73%) ^e	6b (81%) ^d	6b (94%) ^d
7	 S 7	7a (72%) ^e	7b (45%) ^d	7b (65%) ^d
8	 S 8	8a (76%) ^e	8b (98%) ^d	8b (97%) ^d
9	 S 9	9a (33%) ^e	9b (92%) ^d	9b (74%) ^d

10		S 10	10a (72%) ^e	10b (73%) ^d	10b (78%) ^d
11		S 11	11a (82%) ^e	11b (87%) ^d	11b (90%) ^d
12		S 12	12a (85%) ^e	–	–
13		S 13	13a (88%) ^e	13b (53%) ^d	13b (56%) ^d
14		S 14	14a (78%) ^e	14b (24%) ^d	14b (47%) ^d
15		S 15	15a (59%) ^e	15b (53%) ^d	15b (68%) ^d
16		S 16	16a (64%) ^e	16b (46%) ^d	16b (76%) ^d
17		S 17	17a (83%) ^e	17b n.d.	17b n.d.
18		S 18	18a (85%) ^e	18b (9%) ^d	18b (22%) ^d
19		S 19	19a (85%) ^d	19b (76%) ^d	19b (59%) ^d
20		S 20	20a (72%) ^d	20b (88%) ^d	20b (76%) ^d
21		S 21	21a (46%) ^d	21b (87%) ^d	21b (46%) ^d

^a Synthesized according to general procedure A (chap. 5.4.1). ^b Synthesized according to general procedure B (chap. 5.4.2). ^c Synthesized according to general procedure C (chap. 5.4.3). ^d ¹H NMR yield using 1,3,5-trimethoxybenzene as internal standard. ^e Isolated yield after column chromatography.

A considerable difference in the yields was observed for different methods with entry 9. While the ^1H NMR yield of **9a** was 75%, the purification led to a notable product loss, suggesting that the product either degraded upon isolation or didn't come off the column.

Looking at entries 2 and 3, the methoxy substituent on the aromatic ring in ortho position gave better yields as in para position. In case of the heteroaromatic substrates (entries 11-15), **HE 2** was not fully converted into the pyridine form. Probably, longer reaction times would give better yields.

3.4 MECHANISTIC INVESTIGATIONS

3.4.1 CHARACTERIZATION OF THE GROUND STATE

The initial step in any photochemical process involves the absorption of light by a ground state molecule, leading to the formation of an electronically excited state. Therefore, it is crucial to investigate the properties of the substrates in the ground as well as in the excited state. The UV-VIS absorption properties of the Hantzsch ester were described in chapter 3.2.1. To evaluate its redox properties in the ground, electrochemical methods were applied.

Cyclic voltammetry (CV) is the most straightforward method for measuring standard redox potential values. For the CV measurement a solution the Hantzsch ester was imposed to a potential (E) and the resulting current (I) was recorder.

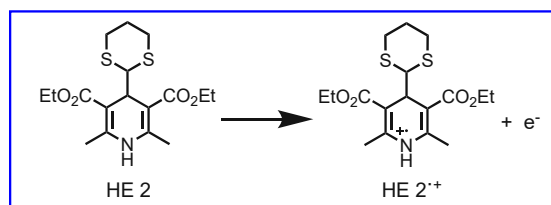


Figure 30: Oxidation of the Hantzsch ester (**HE 2**)

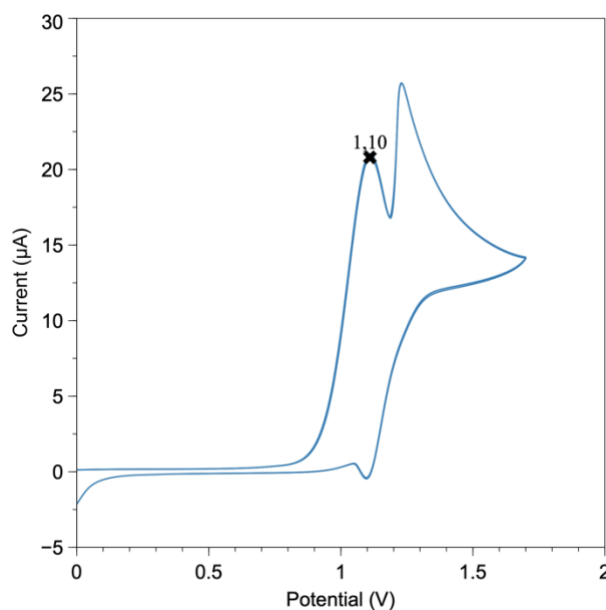
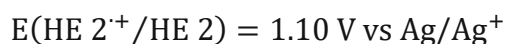


Figure 31: Cyclic voltammogram of **HE 2** relative to Ag/AgCl electrode (3 M KCl); Conditions: 1 mM **HE 2** in 0.1 M $(^n\text{Bu})_4\text{N}[\text{PF}_6]$ in MeCN at 25 °C under exclusion of water and air; scan rate: 100 mV/s

Two oxidation peaks were observed on the cyclic voltammogram (Figure 31). The first peak at a potential of 1.10 V corresponds to the oxidation of the Hantzsch ester as shown in Figure 31. The second peak corresponding to the oxidation of the dithianyl part. The oxidation of **HE 2** is irreversible. If it would be reversible, there would be a negative peak symmetrical to the oxidation peak around 1.0 V. The oxidation of the dithianyl part is quasi-reversible because there is a small negative peak at 1.1 V.



The redox potential of **HE 2** is 1.10 V as written in the equation above.

3.4.2 CHARACTERIZATION OF THE EXCITED STATE

The energy of an excited state of **HE 2** ($E_{0-0}(\text{HE 2}^*/\text{HE 2})$) can be estimated by the energy difference between the lowest vibrational level of the ground state S_0 and the corresponding excited state S_n or T_n . For singlet-excited states, the energy value can be determined spectroscopically. In cases where vibrational structures are absent, E_{0-0} can be approximated from the wavelength that corresponds to the intersection of the absorption and the emission spectrum (Figure 32).^[5] The emission spectrum can be obtained by fluorescence spectroscopy.

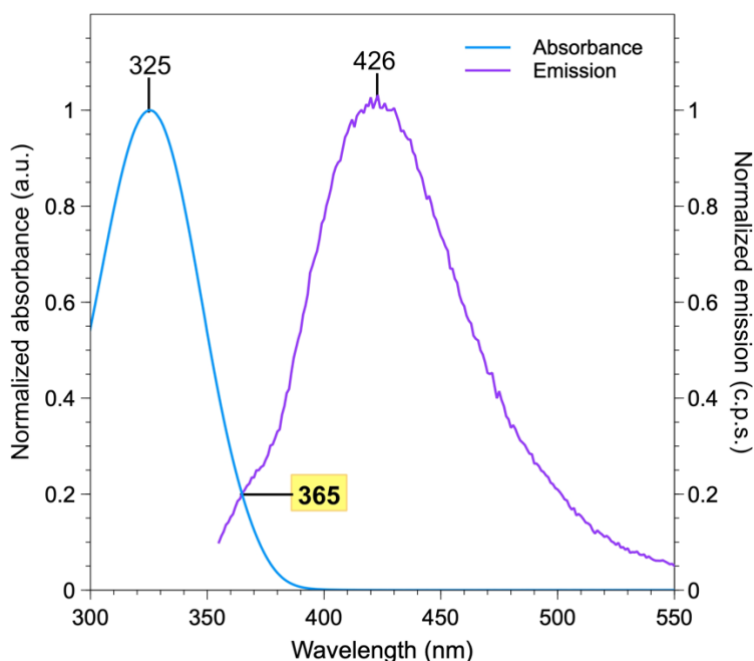


Figure 32: Absorbance and emission spectrum of **HE 2** and their intersection

Blue: Normalized absorption spectrum of the **HE 2**; **Purple:** Normalized emission spectrum of the **HE 2**, excitation wavelength $\lambda=340$ nm; **Conditions** for both measurements: 0.3 mM **HE 2** in MeCN, 10 mm cuvette, 25 °C.

$$E_{0-0}(\text{HE 2}^*/\text{HE 2}) = \frac{h}{e} * \frac{c}{\lambda} = \frac{6.626 * 10^{-34} \text{ C V s}}{1.602 * 10^{-19} \text{ C}} * \frac{3 * 10^8 \frac{\text{m}}{\text{s}}}{365 * 10^{-9} \text{ m}} = 3.40 \text{ V}$$

Calculation of the potential energy from the wavelength gives 3.40 V for the energy of the excited state.

For photochemical reactions proceeding through single-electron transfer (SET), from this energetic value the redox potential of the excited-state species (**HE 2***) can be estimated. A reliable approximation of E^* can be derived from the ground-state redox potential and the energy gap between the ground state and the excited state (Figure 33).^[55]

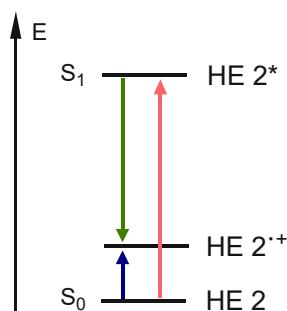


Figure 33: Simplified redox potential diagram

$$\begin{aligned}
 E(\text{HE } 2^{+\cdot} / \text{HE } 2^*) &= E(\text{HE } 2^{+\cdot} / \text{HE } 2) - E_{0-0}(\text{HE } 2^* / \text{HE } 2) = \\
 &= 1.10 \text{ V} - 3.40 \text{ V} = -2.30 \text{ V}
 \end{aligned}$$

The calculation results in a redox potential of -2.3 V for the singlet excited state.

3.4.3 CHARACTERIZATION OF REACTION INTERMEDIATES

3.4.3.1 RADICAL TRAPPING EXPERIMENT

The identification and analysis of highly reactive species that are produced during a photoreaction is essential to understand the underlying mechanism of the process. The simplest approach to confirm the generation of radicals is to capture them and convert them into long-lived intermediates using suitable "traps." A commonly used radical trapping agent is 2,2,6,6-tetramethylpiperidine-1-oxyl (TEMPO).

The radical trapping experiment followed the general procedure B, conducted on a 0.1 mmol scale with the addition of 1 equivalent of TEMPO. The resulting reaction mixture was subjected to GC-MS analysis.

TEMPO adducts (Figure 34) were not detected, likely due to the reduction of TEMPO by the Hantzsch ester (**HE 2**). However, 2,2'-bi-1,3-dithiane was found, indicating its formation through radical-radical recombination of two 1,3-dithiane radicals.

This finding suggests that the dithianyl group undergoes a homolytic cleavage from the Hantzsch ester (**HE 2**) and participates in a radical reaction with the substrate.

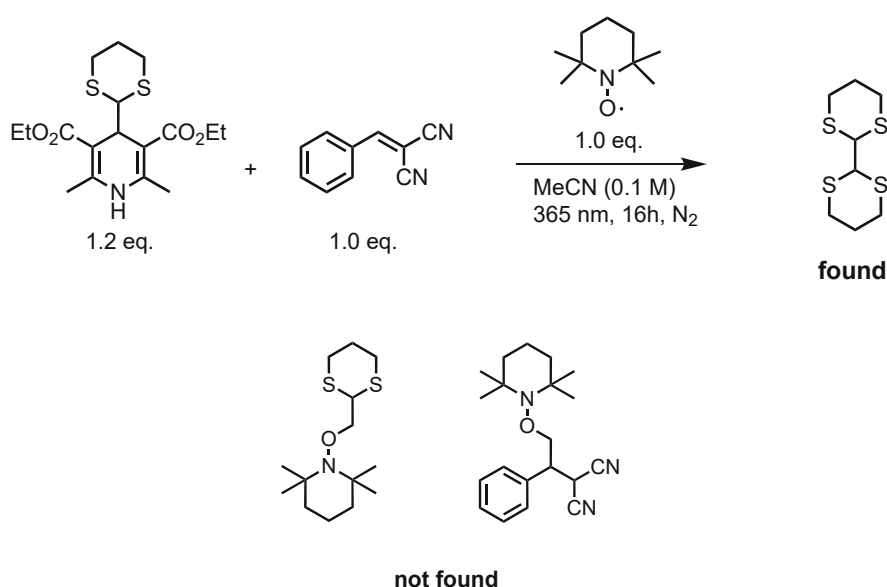


Figure 34: Radical trapping experiment

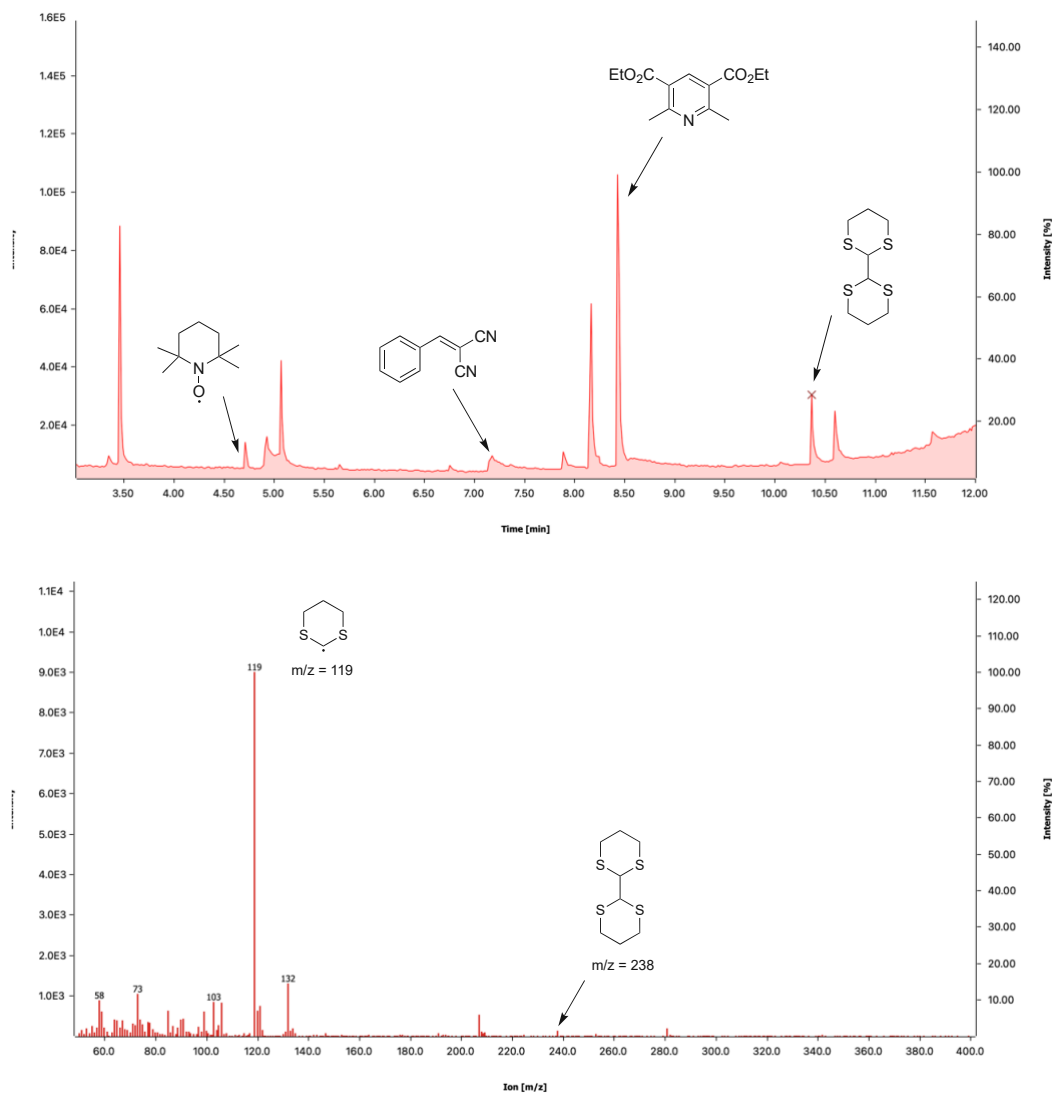


Figure 35: GC-MS spectra of the radical trapping experiment

3.4.3.2 LIGHT ON/OFF EXPERIMENT

Having established that the reaction follows a radical mechanism, the question arises as to whether the reaction is a chain reaction. A light on/off experiment was conducted to answer this question. If the reaction were a chain reaction, it would mean that even in the absence of light, long living radicals are driving the reaction forward. This would manifest as an increase in the yield of the product.

The light on/off experiment followed general procedure B (5.4.2) on a 0.1 mmol scale. After a specified amount of time a sample (20 μL) was taken and the light was either turned on or off (referring to Figure 36). Subsequently, the samples were analysed by GC-FID with calibration using the previously isolated product and dodecanenitrile as the internal standard.

The results undoubtedly demonstrate that no product forms in the absence of light, indicating that there is no chain reaction involved in the product formation.

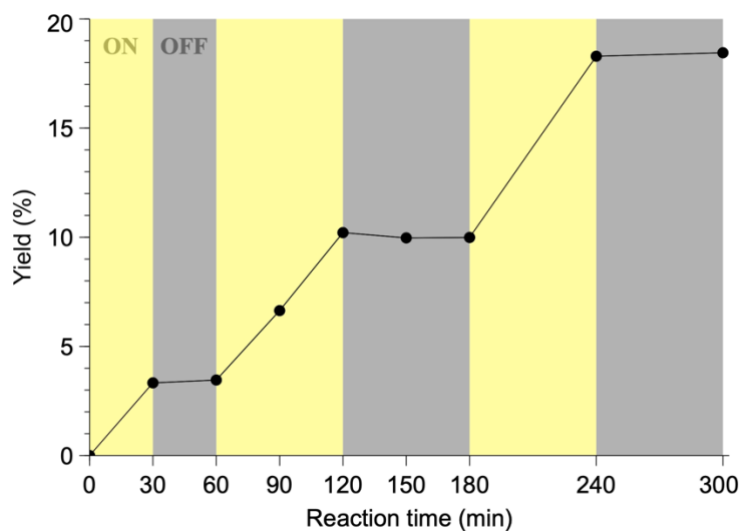


Figure 36: Result of the light on-off experiment

3.4.4 PLAUSIBLE REACTION PATHWAY

The examination of the mechanistic studies led us to the proposal of two plausible mechanistic pathways (Figure 37).

One of the proposed pathways is photolysis. Upon irradiation the 1,3-dithianyl radical is cleaved homolytically from the Hantzsch ester (**HE 2**) and reacts with the substrate, benzylidene malononitrile in a radical recombination. Afterwards a hydrogen atom is transferred to form the product (HAT).

The second proposed pathway is the photoreduction, where the excited Hantzsch ester (**HE 2**) transfers an electron to the substrate (SET), then the 1,3-dithianyl group is cleaved homolytically. Afterwards, the radical recombination of the cleaved radical and the substrate takes place followed by a proton transfer to form the product and the oxidized Hantzsch ester.

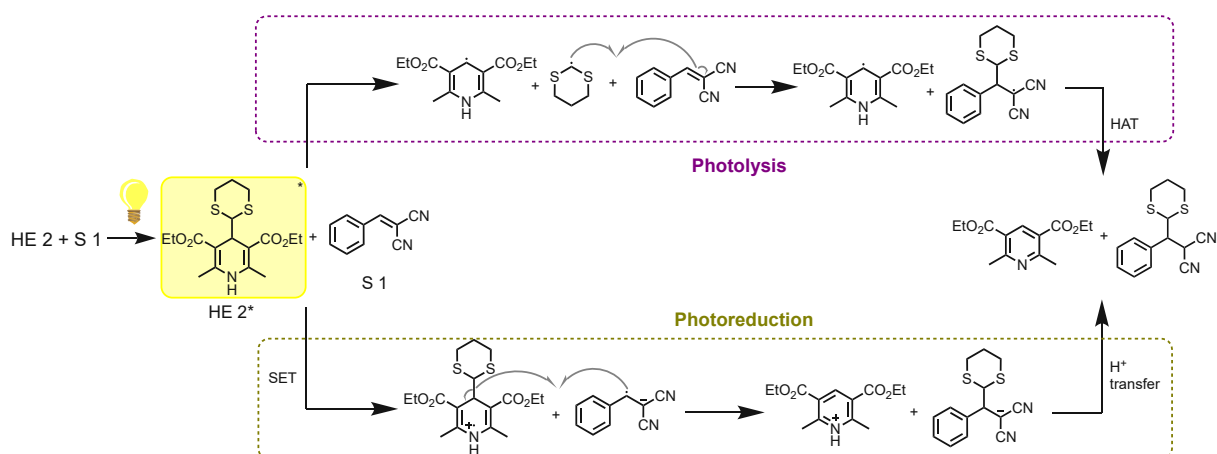


Figure 37: Proposed mechanistic pathways for the model reaction

Considering that the Hantzsch ester (**HE 2**) is a strong reductant in the excited state and comparing its redox potential with the redox potential of the benzylidene malononitrile from the literature^[56], a reduction of the malononitrile substrate by the **HE 2** is very much possible, making the photoreduction a thermodynamically feasible mechanistic pathway.

Table 8: Comparison of the redox potentials

Compound	Redox potential E (V) (vs Ag/Ag ⁺)
Benzylidene malononitrile (CN ₂ /CN ₂ ^{•-})	-1,4
Hantzsch ester (HE 2 ^{•+} /HE 2 [*])	-2,3

4 CONCLUSION AND OUTLOOK

In this work, a method was successfully developed for the transfer of acetal groups from Hantzsch ester radical reservoirs to activated olefines under photochemical conditions. Experiments were conducted to unravel the photochemical properties of the Hantzsch esters, as well as the overall reaction. A comprehensive analysis of various components in the reaction setup, such as the light source and temperature control methods, revealed no discernible differences for the model reaction under these conditions.

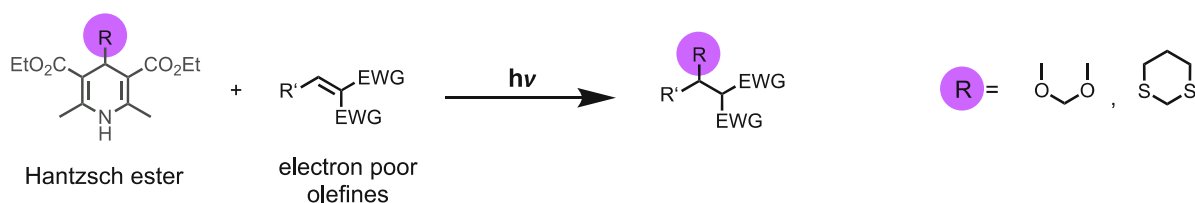


Figure 38: Hantzsch esters as acetal group transfer-agents under photochemical conditions

Following systematic optimization, the broad substrate scope of 21 different electron acceptors with three different methodologies was explored. Mechanistic studies and control experiments were carried out to gain deeper insights into both the ground and excited states of the Hantzsch ester, thereby elucidating potential mechanistic pathways.

While photoreactions exhibited noteworthy efficacy, the prospect of optimizing the process for flow reactions emerged as an enticing next step. Considering the potential advantages of flow reactions, the upscaling of the current method to a flow reactor represents an intriguing avenue for future research.

5 EXPERIMENTAL SECTION

5.1 MATERIALS AND METHODS

All chemicals purchased from commercial suppliers were used without further purification unless otherwise noted. Dry solvents intended for anhydrous reactions were pre-distilled and desiccated on Al₂O₃ columns (PURESOLV, Innovative Technology).

Nuclear magnetic resonance (NMR) spectroscopy: ¹H NMR, ¹³C NMR and ¹⁹F NMR were used for purity and structure determination of products. NMR spectral data were collected on a Bruker Avance 400 (400 MHz for ¹H; 101 MHz for ¹³C) spectrometer, or a Bruker Avance I 500 (500 MHz for ¹H; 126 MHz for ¹³C), or a Bruker Avance III HD 600 (600 MHz for ¹H; 151 MHz for ¹³C ;565 MHz for ¹⁹F) spectrometer at 20 °C. Chemical shifts are reported in δ/ppm, coupling constants J are given in Hertz. Solvent residual peaks were used as internal standard for all NMR measurements. The quantification of ¹H cores was obtained from integrations of appropriate resonance signals. Abbreviations used in NMR spectra: s – singlet, d – doublet, t – triplet, q – quartet, m – multiplet, dd – doublet of doublet.

Low-resolution mass spectrometry (LRMS) was carried out on an Agilent 6890N GC-System with 5975 MS mass detector and H₂ as carrier gas.

High resolution mass spectrometry (HRMS) was carried out by the Central Analytics at the department of chemistry, University of Hamburg. Abbreviations used in MS spectra: M – molar mass of target compound, ESI – electrospray ionization.

Column chromatography: TLC was performed on the commercial SiO₂-coated aluminium plates (DC60 F254, Merck) or on Alox N plates (60 F254, Merck). Visualization was done by UV light (254 nm). Isolated products were purified by column chromatography on silica gel (Acros Organics, mesh 35-70, 60 Å pore size) or on Alox N (mesh 50-200, 90 Å pore size).

GC yields were determined by using an Agilent Technologies 7820A system with an FID detector.

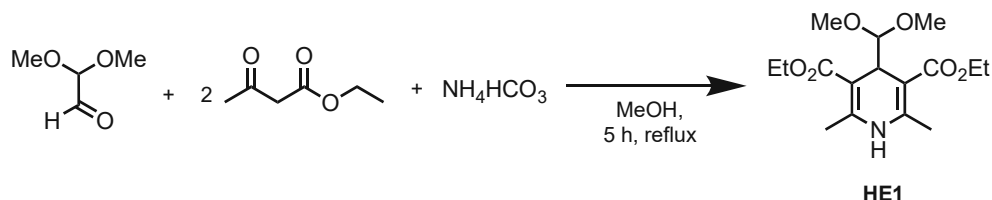
Cyclic voltammetry (CV) measurements were performed with a potentiostat galvanostat PGSTAT101 from Metrohm Autolab using a glassy carbon working electrode, a platinum wire counter electrode, a silver/silver(I)chloride reference electrode and $N(n\text{-Bu})_4\text{PF}_6$ (0.1 M) as supporting electrolyte. The potentials were achieved relative to the Fc/Fc^+ redox couple with ferrocene as external standard.

UV/VIS absorption spectroscopy was performed at room temperature on an Agilent Cary 5000 UV/VIS NIR double beam spectrometer with a 10 mm quartz cuvette.

The fluorescence spectra were recorded at room temperature using an Agilent Cary Eclipse Fluorescence Spectrophotometer in quartz cuvettes fitted with a rubber septum. The excitation slit was opened to 5 nm and the emission slit to 10 nm.

5.2 SYNTHESIS OF HANTZSCH ESTERS

5.2.1 SYNTHESIS OF DIETHYL 4-(DIMETHOXYMETHYL)-2,6-DIMETHYL-1,4-DIHYDROPYRIDINE-3,5-DICARBOXYLATE (**HE 1**)



Dimethoxyacetaldehyde (60% in H₂O; 4.3 g, 25 mmol, 1.0 eq.), ethyl acetoacetate (6.5 g, 50 mmol, 2.0 eq.) and ammonium bicarbonate (2.0 g, 25 mmol, 1.0 eq.) were stirred and refluxed in methanol (25 mL, 1.0 M) for 5 hours. The mixture was dried *in vacuo* and the crude product was recrystallized from diethyl ether to form a lightly yellow powder (5.5 g, 17 mmol, 67%).

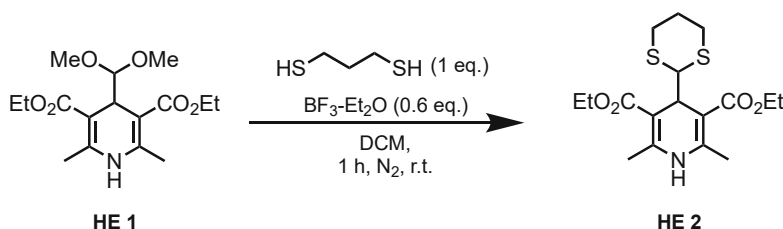
¹H NMR (500 MHz, CDCl₃) δ 5.68 (s, 1H), 4.35 (d, *J* = 5.2 Hz, 1H), 4.27 – 4.10 (m, 4H), 3.96 (d, *J* = 5.2 Hz, 1H), 3.30 (s, 6H), 2.29 (s, 6H), 1.29 (t, *J* = 7.1 Hz, 6H).

¹³C NMR (101 MHz, CDCl₃) δ 168.39, 145.01, 107.93, 99.29, 59.82, 55.33, 36.91, 19.47, 14.52.

Analytical data is in accordance to literature. ^[48]

5.2.2 SYNTHESIS OF DIETHYL 4-(1,3-DITHIAN-2-YL)-2,6-DIMETHYL-1,4-DIHYDROPYRIDINE-3,5-DICARBOXYLATE (**HE 2**)

5.2.2.1 METHOD 1



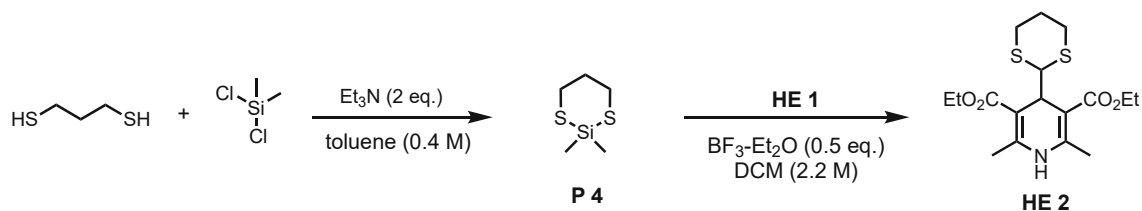
To a solution of diethyl 4-(dimethoxymethyl)-2,6-dimethyl-1,4-dihydropyridine-3,5-dicarboxylate (**HE 1**, 3.1 g, 9.4 mmol) and 1,3-propanedithiol (1.0 g, 9.4 mmol) in methylene chloride (108 mL, 0.1 M) boron trifluoride diethyl etherate (0.8 g, 0.6 mmol) was added dropwise *via* syringe under nitrogen atmosphere. After 1 hour of stirring at room temperature TLC showed full conversion of the starting material so the reaction was quenched with water, followed by an extraction with saturated NaHCO₃ solution, then with brine. The combined organic phases were dried over anhydrous Na₂SO₄ and the solvent was removed by rotary evaporation. The residue was washed with diethyl ether and the product (2.6 g, 6.9 mmol, 74%) was obtained as a colourless powder.

¹H NMR (600 MHz, CDCl₃) δ 5.84 (s, 1H), 4.66 (d, *J* = 8.6 Hz, 1H), 4.23 (q, *J* = 7.1 Hz, 4H), 3.35 (d, *J* = 8.6 Hz, 1H), 3.05 – 2.93 (m, 2H), 2.65 – 2.52 (m, 2H), 2.37 (s, 6H), 2.02 – 1.95 (m, 2H), 1.33 (t, *J* = 7.1 Hz, 6H).

¹³C NMR (101 MHz, CDCl₃) δ 168.45, 168.05, 144.45, 144.00, 102.68, 60.10, 60.05, 51.16, 36.77, 28.09, 26.29, 26.26, 19.75, 19.72, 19.64, 14.59, 14.56.

HRMS (ESI): *m/z* = calcd. for C₁₇H₂₅NO₄S₂Na [M + Na]⁺: 394.1117, found: 394.1129; [2M+Na]⁺: 765.2342, found: 765.2352; [M + K]⁺: 410.0857, found: 410.0860.

5.2.2.2 METHOD 2



a) Synthesis of 2,2-dimethyl-1,3,2-dithiasilane (**P 4**) according to literature procedure.^[57]

To a mixture of 1,3-propanedithiol (1.3 g, 12 mmol) and triethylamine (2.4 g, 24 mmol) in toluene (0.4 M), dimethyldichlorosilane (1.5 g, 12 mmol) was added *via* syringe. Triethylammonium hydrochloride precipitated immediately as a white solid. The mixture was refluxed for 3 hours then the filtered yellow liquid was concentrated *in vacuo*. The product was purified by distillation (b.p. 81 °C, 12 mbar) to give a slightly yellow liquid (1.2 g, 62%).

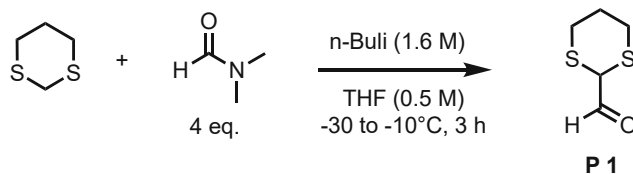
¹H NMR (400 MHz, CDCl₃) δ 2.85 – 2.72 (m, 4H), 2.03 – 1.91 (m, 2H), 0.59 (s, 6H).

Analytical data is in accordance to literature. ^[57]

b) Synthesis of **HE 2** according to literature procedure.^[52]

To a stirred mixture of 2,2-dimethyl-2-sila-1,3-dithiane (0.6 g, 3.8 mmol) and **HE 1** (1.3 g, 3.8 mmol) in DCM (2.2 M) at 0 °C was added BF₃-OEt₂ (0.3 g, 1.9 mmol) dropwise. The mixture turned from colourless to yellow and upon a few seconds a bulk was formed. After the addition was completed, KF solution (1.4 mL, 1.0 M) was added. The solid was filtered off and washed with cold diethyl ether twice upon which the colour of the product changed from yellow to white (654 mg, 46%).

Analytical data same as in Method 1 (5.2.2.1).

5.2.3 UNSUCCESSFUL SYNTHESIS OF **HE 2**5.2.3.1 SYNTHESIS OF 2-FORMYL-1,3-DITHIANE (**P 1**)

Synthesized by following literature procedure.^[58]

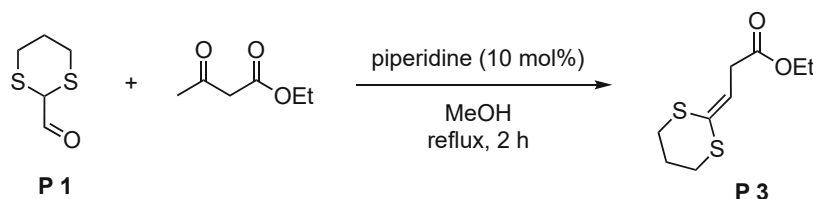
A solution containing 1,3-dithiane (6,0 g, 50 mmol) in anhydrous tetrahydrofuran (100 mL, 0.5 M) was cooled with stirring under nitrogen to -30 °C (dry ice and acetone bath) and treated dropwise with 1.6 M butyllithium in hexane (3.2 g, 50 mmol). After 1 hour of additional stirring the solution was transferred by syringe and added dropwise to a flask containing previously cooled (-10 °C) dimethylformamide (15 mL, 200 mmol). The mixture was allowed to stir for 2 hours at -10 °C and then stored overnight at 5 °C.

The resulting suspension was poured into ice water and the mixture was extracted 3 times with pentane. The aqueous layer was neutralized with diluted (1 N) hydrochloric acid and then extracted three times with ether. The organic extracts were dried (MgSO₄) and concentrated to a yellow oil, which was distilled (b.p. 105 °C, 5 mbar) to give the desired compound (**P 2**) as a pale-yellow liquid (2.2 g, 30%).

The product was stored at -20 °C to prevent dimerization.

¹H NMR (400 MHz, CDCl₃) δ 9.51 (d, *J* = 1.1 Hz, 1H), 4.10 (s, 1H), 3.11 – 2.96 (m, 2H), 2.62 – 2.49 (m, 2H), 2.14 – 1.90 (m, 2H).

Analytical data was in accordance with literature.^[58]

5.2.3.2 SYNTHESIS OF ETHYL 3-(1,3-DITHIAN-2-YLIDENE)PROPANOATE (**P 3**)

Synthesized by following literature procedure.^[59]

To a solution of 2-formyl-1,3-dithiane (**P 1**, 1.0 g, 6.8 mmol) in methanol (14 mL), piperidine (58 mg, 0.7 mmol) and ethyl acetoacetate (0.88 g, 6.8 mmol) were added at room temperature. The reaction mixture was refluxed for 2.5 hours. Afterwards, the solvent was evaporated under reduced pressure and the yellow crude product was purified by column chromatography (Alox N, 5:1 pentane:EtOAc) to obtain a yellow oily product (**P 3**, 544 mg, 31%).

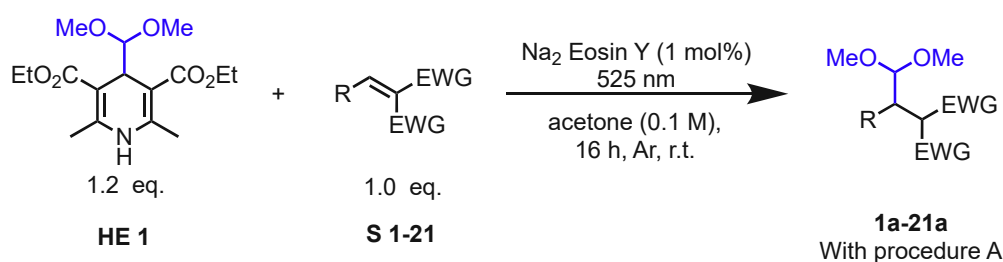
¹H NMR (600 MHz, CDCl₃) δ 6.07 (t, *J* = 7.1 Hz, 1H), 4.14 (q, *J* = 7.1 Hz, 2H), 3.27 (d, *J* = 7.0 Hz, 2H), 2.97 – 2.78 (m, 4H), 2.16 (tt, *J* = 7.8, 5.1 Hz, 2H), 1.26 (t, *J* = 7.1 Hz, 3H).

¹³C NMR (151 MHz, CDCl₃) δ 171.02, 130.53, 124.01, 60.97, 34.91, 30.07, 29.49, 28.35, 24.95, 14.34.

5.3 ACETALIZATION OF OLEFINS UNDER PHOTOCHEMICAL CONDITIONS

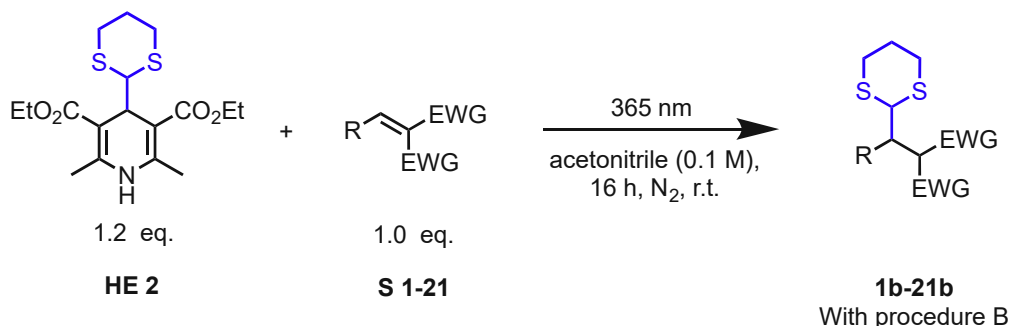
5.4 GENERAL PROCEDURES

5.4.1 GENERAL PROCEDURE A



To a 4 mL screw cap vial equipped with a stir bar, diethyl 4-(dimethoxymethyl)-2,6-dimethyl-1,4-dihydropyridine-3,5-dicarboxylate (**HE 1**, 0.12 mmol, 1.2 equiv.), the substrate (**S 1-21**, 0.10 mmol, 1.0 equiv.) and Eosin Y disodium salt (1 mol%) were added. Acetone (1.0 mL, 0.10 M) was added in the glove box and the vial was sealed with a plastic screw cap. The vial was placed in a commercial reactor with water cooling (25 °C) and fitted with a green LED light source ($\lambda_{\text{max}} = 525\text{-}530 \text{ nm}$, 10 mW/cm²) from EvoluChem. The reaction was stirred at room temperature for 16 hours. Afterwards, the mixture was concentrated *in vacuo* and the residue was purified by column chromatography (Alox N or SiO₂, appropriate mixture of pentane/ethyl acetate or diethyl ether) to afford the corresponding products **1a-21a**.

5.4.2 GENERAL PROCEDURE B

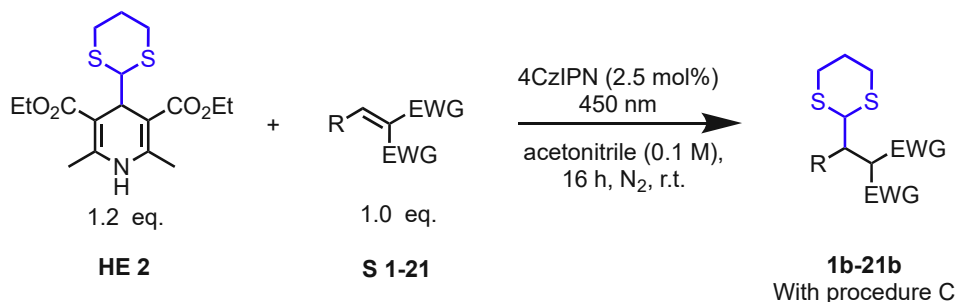


To a 4 mL screw cap vial equipped with a stir bar, diethyl 4-(1,3-dithian-2-yl)-2,6-dimethyl-1,4-dihydropyridine-3,5-dicarboxylate (**HE 2**, 0.12 mmol, 1.2 equiv.) and the substrate (**S 1-21**, 0.10 mmol, 1.0 equiv.) were added. The vial was sealed with a septum screw cap, evacuated, and filled back with nitrogen. Acetonitrile (1.0 mL, 0.10 M) was added *via* a syringe. The vial was placed into the photoreactor (EvoluChem) with water cooling (25 °C). The reaction mixture was stirred for 16 hours under UV light irradiation ($\lambda_{\text{max}}=365\text{ nm}$, 15 mW/cm^2 , LED from EvoluChem). Afterwards the mixture was concentrated *in vacuo*.

To determine the yields of **1b-21b**, ^1H NMR measurement was applied by adding 1,3,5-trimethoxybenzene as internal standard.

To isolate the corresponding products, the residues were purified by column chromatography (Alox N or SiO_2 , appropriate mixture of pentane/ethyl acetate), affording the corresponding products **1b-21b**.

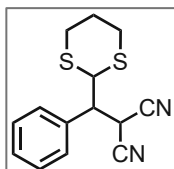
5.4.3 GENERAL PROCEDURE C



To a 4 mL screw cap vial equipped with a stir bar, diethyl 4-(1,3-dithian-2-yl)-2,6-dimethyl-1,4-dihydropyridine-3,5-dicarboxylate (**HE 2**, 0.12 mmol, 1.2 equiv.), the substrate (**S 1-21**, 0.10 mmol, 1.0 equiv.) and the photocatalyst 4CzIPN (2.5 mol%) were added. The vial was sealed with a septum screw cap, evacuated, and filled back with nitrogen. Acetonitrile (1.0 mL, 0.10 M) was added *via* a syringe. The vial was placed in a commercial reactor (EvoluChem) with water cooling (25 °C) and fitted with a blue LED light source ($\lambda_{\text{max}} = 450 \text{ nm}$, 55 mW/cm^2) from EvoluChem. The reaction mixture was stirred for 16 hours. Afterwards the mixture was concentrated *in vacuo*. The yields of **1b-21b** were determined by ^1H NMR measurement by adding 1,3,5-trimethoxybenzene as internal standard.

5.5 ISOLATED COMPOUNDS

5.5.1 2-((1,3-DITHIAN-2-YL)(PHENYL)METHYL)MALONONITRILE (**1B**)

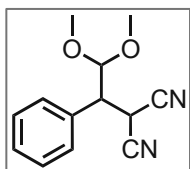


Starting from benzylidene malononitrile (**S 1**) and following the general procedure B. Purified by column chromatography (Alox N, petroleum ether/EtOAc, 3:1, $R_f=0.39$). Pale yellow oil (24 mg, 86%).

$^1\text{H NMR}$ (400 MHz, CDCl_3) δ 7.57 – 7.31 (m, 5H), 4.75 (d, $J = 5.8$ Hz, 1H), 4.51 (d, $J = 10.1$ Hz, 1H), 3.70 – 3.39 (m, 1H), 3.11 – 2.66 (m, 4H), 2.22 – 2.05 (m, 1H), 2.03 – 1.86 (m, 1H).

$^{13}\text{C NMR}$ (101 MHz, CDCl_3) δ 133.56, 129.87, 129.29, 128.64, 111.77, 111.23, 50.29, 47.56, 29.60, 29.41, 27.87, 25.15.

5.5.2 2-(2,2-DIMETHOXY-1-PHENYLETHYL)MALONONITRILE (**1A**)



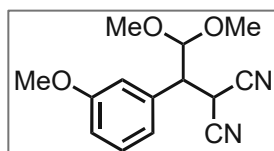
Starting from benzylidene malononitrile (**S 1**) and following the general procedure A. Purified by column chromatography (Alox N, pentane/EtOAc, 5:1, $R_f=0.39$). Pale yellow oil (19 mg, 84%).

$^1\text{H NMR}$ (400 MHz, CDCl_3) δ 7.42 (s, 5H), 4.81 (d, $J = 6.6$ Hz, 1H), 4.34 (d, $J = 5.6$ Hz, 1H), 3.52 (s, 3H), 3.43 (t, $J = 6.1$ Hz, 1H), 3.31 (s, 3H).

$^{13}\text{C NMR}$ (101 MHz, CDCl_3) δ 133.55, 129.34, 128.87, 112.07, 111.95, 104.38, 56.46, 55.11, 49.25, 25.96.

HRMS (ESI): $m/z = \text{cald. for } \text{C}_{13}\text{H}_{15}\text{N}_2\text{O}_2 \text{ [M + H]}^+$: 231.1128, found: 231.1128

5.5.3 2-(2,2-DIMETHOXY-1-(3-METHOXYPHENYL)ETHYL) MALONONITRILE (**2A**)



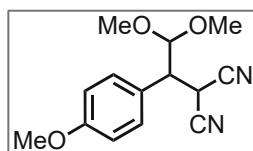
Starting from 2-(2-methoxybenzylidene)malononitrile (**S 2**) and following the general procedure A. Purified by column chromatography (Alox N, pentane/EtOAc, 4:1, $R_f=0.22$). Pale yellow oil (23 mg, 86%).

$^1\text{H NMR}$ (500 MHz, CDCl_3) δ 7.34 (t, $J = 7.8$ Hz, 1H), 6.99 (d, $J = 8.5$ Hz, 1H), 6.97 – 6.85 (m, 2H), 4.78 (d, $J = 6.6$ Hz, 1H), 4.32 (d, $J = 5.6$ Hz, 1H), 3.83 (s, 3H), 3.52 (s, 3H), 3.39 (t, $J = 6.2$ Hz, 1H), 3.32 (s, 3H).

$^{13}\text{C NMR}$ (126 MHz, CDCl_3) δ 160.11, 135.03, 130.39, 120.99, 114.77, 114.55, 112.06, 112.01, 104.43, 56.48, 55.41, 55.21, 49.23, 25.88.

HRMS (ESI): $m/z = \text{cald. for } \text{C}_{14}\text{H}_{17}\text{N}_2\text{O}_3 [\text{M} + \text{H}]^+$: 261.1234, found: 261.1236

5.5.4 2-(2,2-DIMETHOXY-1-(4-METHOXYPHENYL)ETHYL) MALONONITRILE (**3A**)



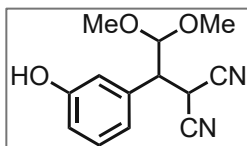
Starting from 2-(4-methoxybenzylidene)malononitrile (**S 3**) and following the general procedure A. Purified by column chromatography (Alox N, pentane/EtOAc, 5:1, $R_f=0.44$). Off-white solid (21 mg, 80%, $T_m=57-58$ °C)

$^1\text{H NMR}$ (500 MHz, CDCl_3) δ 7.34 (d, $J = 8.7$ Hz, 2H), 6.94 (d, $J = 8.7$ Hz, 2H), 4.76 (d, $J = 6.7$ Hz, 1H), 4.31 (d, $J = 5.5$ Hz, 1H), 3.82 (s, 3H), 3.51 (s, 3H), 3.38 (t, 1H), 3.31 (s, 3H).

$^{13}\text{C NMR}$ (126 MHz, CDCl_3) δ 160.23, 130.05, 125.42, 114.70, 112.21, 112.04, 104.43, 56.43, 55.39, 55.00, 48.61, 26.19.

HRMS (ESI): $m/z = \text{cald. for } \text{C}_{14}\text{H}_{17}\text{N}_2\text{O}_3 [\text{M} + \text{H}]^+$: 261.1234, found: 261.1250

5.5.5 2-(1-(3-HYDROXYPHENYL)-2,2-DIMETHOXYETHYL) MALONONITRILE (**4A**)

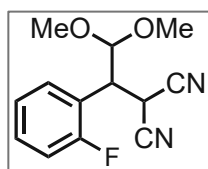


Starting from 2-(3-hydroxybenzylidene)malononitrile (**S 4**) and following the general procedure A. Purified by flash column chromatography (Alox N, pentane/EtOAc, 3:1, EtOAc, $R_f=0.39$). Pale yellow oil (19 mg, 84%).

$^1\text{H NMR}$ (400 MHz, CDCl_3) δ 7.35 – 7.17 (m, 1H), 7.02 – 6.70 (m, 3H), 4.75 (d, $J = 6.6$ Hz, 1H), 4.31 (d, $J = 5.7$ Hz, 1H), 3.50 (s, 3H), 3.36 (t, $J = 5.8$ Hz, 1H), 3.31 (s, 3H), 2.26 (s, 1H).

$^{13}\text{C NMR}$ (126 MHz, CDCl_3) δ 135.72, 132.59, 132.07, 130.83, 127.53, 123.30, 111.79, 111.65, 104.21, 56.65, 55.47, 48.93, 25.67.

5.5.6 2-(1-(2-FLUOROPHENYL)-2,2-DIMETHOXYETHYL) MALONONITRILE (**5A**)



Starting from 2-(2-fluorobenzylidene)malononitrile (**S 5**) and following the general procedure A. Purified by column chromatography (Alox N, pentane/EtOAc, 4:1, $R_f=0.53$). Colourless oil (15 mg, 60%).

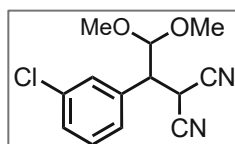
$^1\text{H NMR}$ (400 MHz, CDCl_3) δ 7.56 – 7.49 (m, 1H), 7.43 – 7.36 (m, 1H), 7.25 – 7.12 (m, 2H), 4.83 (d, $J = 6.7$ Hz, 1H), 4.34 (d, $J = 6.2$ Hz, 1H), 3.96 (t, $J = 6.5$ Hz, 1H), 3.52 (s, 3H), 3.33 (s, 3H).

$^{13}\text{C NMR}$ (126 MHz, CDCl_3) δ 162.08, 160.11, 131.00, 129.35, 125.07, 120.97, 116.35, 111.79, 103.71, 56.40, 54.53, 41.22, 25.14.

$^{19}\text{F NMR}$ (565 MHz, CDCl_3) δ -114.17 – -119.41 (m).

HRMS (ESI): $m/z = \text{calcd. for } \text{C}_{13}\text{H}_{14}\text{FN}_2\text{O}_2 \text{ [M + H]}^+$: 249.1034, found: 249.1050

5.5.7 2-(1-(3-CHLOROPHENYL)-2,2-DIMETHOXYETHYL) MALONONITRILE (6A)



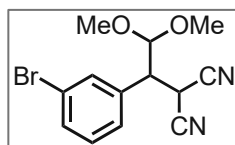
Starting from 2-(3-chlorobenzylidene)malononitrile (**S 6**) and following the general procedure A. Purified by column chromatography (Alox N, pentane/EtOAc, 4:1, $R_f=0.44$). Colourless oil (19 mg, 73%).

$^1\text{H NMR}$ (400 MHz, CDCl_3) δ 7.44 – 7.29 (m, 4H), 4.76 (d, $J = 6.4$ Hz, 1H), 4.33 (d, $J = 5.9$ Hz, 1H), 3.52 (s, 3H), 3.40 (t, $J = 6.2$ Hz, 1H), 3.34 (s, 3H).

$^{13}\text{C NMR}$ (126 MHz, CDCl_3) δ 135.47, 135.21, 130.59, 129.66, 129.18, 127.10, 111.80, 111.67, 104.22, 56.64, 55.46, 48.98, 25.67.

HRMS (ESI): $m/z = \text{cald. for } \text{C}_{13}\text{H}_{14}\text{ClN}_2\text{O}_2 \text{ [M + H]}^+$: 265.0739, found: 265.0713

5.5.8 2-(1-(3-BROMOPHENYL)-2,2-DIMETHOXYETHYL) MALONONITRILE (7A)



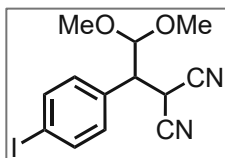
Starting from 2-(3-bromobenzylidene)malononitrile (**S 7**) and following the general procedure A. Purified by column chromatography (Alox N, pentane/EtOAc, 4:1, $R_f=0.37$). Colourless oil (22 mg, 72%).

$^1\text{H NMR}$ (400 MHz, CDCl_3) δ 7.61 – 7.52 (m, 2H), 7.40 – 7.27 (m, 2H), 4.76 (d, $J = 6.3$ Hz, 1H), 4.33 (d, $J = 5.9$ Hz, 1H), 3.52 (s, 3H), 3.39 (t, $J = 6.2$ Hz, 1H), 3.34 (s, 3H).

$^{13}\text{C NMR}$ (126 MHz, CDCl_3) δ 135.72, 132.59, 132.07, 130.83, 127.53, 123.30, 111.79, 111.65, 104.21, 56.65, 55.47, 48.93, 25.67.

HRMS (ESI): $m/z = \text{cald. for } \text{C}_{13}\text{H}_{14}\text{BrN}_2\text{O}_2 \text{ [M + H]}^+$: 309.0233, found: 309.0193

5.5.9 2-(1-(4-iodophenyl)-2,2-dimethoxyethyl)malononitrile (8A)



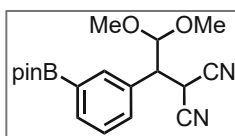
Starting from 2-(4-iodobenzylidene)malononitrile (**S 8**) and following the general procedure A. Purified by column chromatography (Alox N, pentane/EtOAc, 4:1, $R_f=0.36$). Pale yellow solid (28 mg, 76%, $T_m=60-61$ °C).

$^1\text{H NMR}$ (400 MHz, CDCl_3) δ 7.76 (d, $J = 8.4$ Hz, 2H), 7.16 (d, $J = 8.4$ Hz, 2H), 4.75 (d, $J = 6.5$ Hz, 1H), 4.32 (d, $J = 5.7$ Hz, 1H), 3.51 (s, 3H), 3.37 (t, $J = 6.1$ Hz, 1H), 3.32 (s, 3H).

$^{13}\text{C NMR}$ (101 MHz, CDCl_3) δ 138.48, 133.09, 130.73, 111.86, 111.69, 104.08, 95.46, 56.58, 55.31, 48.94, 25.69.

HRMS (ESI): $m/z = \text{cald. for } \text{C}_{13}\text{H}_{14}\text{IN}_2\text{O}_2 [\text{M} + \text{H}]^+$: 357.0095, found: 357.0080

5.5.10 2-(2,2-dimethoxy-1-(3-(4,4,5,5-tetramethyl-1,3,2-dioxaborolan-2-yl)phenyl)ethyl)malononitrile (9A)



Starting from 2-(3-(4,4,5,5-tetramethyl-1,3,2-dioxaborolan-2-yl)benzylidene)malononitrile (**S 9**) and following the general procedure A. Purified by column chromatography (SiO_2 ,

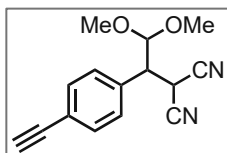
pentane/EtOAc, 5:1 \rightarrow 1:1, 1% Et_3N , $R_f=0.24$ and baseline). Colourless oil (12 mg, 33%).

$^1\text{H NMR}$ (400 MHz, CDCl_3) δ 7.87 – 7.80 (m, 1H), 7.78 – 7.73 (m, 1H), 7.57 – 7.50 (m, 1H), 7.43 (t, $J = 7.6$ Hz, 1H), 4.81 (d, $J = 6.5$ Hz, 1H), 4.33 (d, $J = 6.0$ Hz, 1H), 3.52 (s, 3H), 3.46 (t, $J = 6.2$ Hz, 1H), 3.31 (s, 3H), 1.35 (s, 12H).

$^{13}\text{C NMR}$ (126 MHz, CDCl_3) δ 135.75, 135.51, 133.03, 131.09, 128.70, 112.06, 112.01, 104.46, 84.17, 56.52, 55.03, 49.23, 25.79, 25.04.

HRMS (ESI): $m/z = \text{cald. for } \text{C}_{19}\text{H}_{25}\text{BN}_2\text{O}_4 [\text{M} + \text{Na}]^+$: 379.1799, found: 379.1808; $[\text{2M} + \text{Na}]^+$: 735.3706, found: 735.3719

5.5.11 2-(1-(4-ETHYNYLPHENYL)-2,2-DIMETHOXYETHYL)
MALONONITRILE (**10A**)



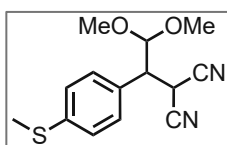
Starting from 2-(4-ethynylbenzylidene)malononitrile (**S 10**) and following the general procedure A. Purified by column chromatography (Alox N, pentane/EtOAc, 4:1, $R_f=0.26$). Colourless oil (18 mg, 72%).

$^1\text{H NMR}$ (400 MHz, CDCl_3) δ 7.55 (d, $J = 8.4$ Hz, 2H), 7.39 (d, $J = 8.3$ Hz, 2H), 4.78 (d, $J = 6.6$ Hz, 1H), 4.34 (d, $J = 5.7$ Hz, 1H), 3.52 (s, 3H), 3.42 (t, $J = 6.2$ Hz, 1H), 3.31 (s, 3H), 3.13 (s, 1H).

$^{13}\text{C NMR}$ (126 MHz, CDCl_3) δ 134.10, 133.00, 128.96, 123.39, 111.88, 111.74, 104.24, 82.86, 78.64, 56.55, 55.36, 49.18, 25.72.

HRMS (ESI): $m/z = \text{cald. for } \text{C}_{15}\text{H}_{15}\text{N}_2\text{O}_2$ $[\text{M} + \text{H}]^+$: 277.1005, found: 277.1010; $[\text{M} + \text{Na}]^+$: 255.1128, found: 255.1120; $[\text{M} + \text{Na}]^+$: 277.0947, found: 277.0960

5.5.12 2-(2,2-DIMETHOXY-1-(4-(METHYLTHIO)PHENYL)ETHYL)
MALONONITRILE (**11A**)



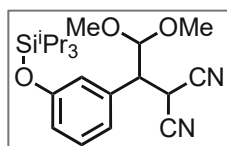
Starting from 2-(4-(methylthio)benzylidene)malononitrile (**S 11**) and following the general procedure A. Purified by column chromatography (Alox N, pentane/EtOAc, 4:1, $R_f=0.38$). Off-white solid (23 mg, 82%, $T_m=67-68$ °C).

$^1\text{H NMR}$ (400 MHz, CDCl_3) δ 7.38 – 7.24 (m, 4H), 4.77 (d, $J = 6.6$ Hz, 1H), 4.32 (d, $J = 5.6$ Hz, 1H), 3.51 (s, 3H), 3.38 (dd, $J = 6.7, 5.6$ Hz, 1H), 3.31 (s, 3H), 2.49 (s, 3H).

$^{13}\text{C NMR}$ (101 MHz, CDCl_3) δ 140.29, 129.82, 129.25, 126.75, 112.06, 111.90, 104.25, 56.48, 55.10, 48.81, 25.97, 15.42.

HRMS (ESI): $m/z = \text{cald. for } \text{C}_{14}\text{H}_{17}\text{N}_2\text{O}_2\text{S}$ $[\text{M} + \text{H}]^+$: 277.1005, found: 277.1010; $[\text{M} + \text{Na}]^+$: 299.0824, found: 299.0827

5.5.13 2-(2,2-DIMETHOXY-1-(3-((TRIIISOPROPYLSILYL)OXY)PHENYL)ETHYL)MALONONITRILE (**12A**)



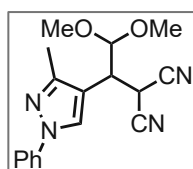
Starting from 2-(3-((triisopropylsilyl)oxy)benzylidene)malononitrile (**S 12**) and following the general procedure A. Purified by column chromatography (Alox N, pentane/EtOAc, 10:1, $R_f=0.28$). Colourless oil (38 mg, 85%).

$^1\text{H NMR}$ (500 MHz, CDCl_3) δ 7.31 – 7.19 (m, 1H), 7.01 – 6.95 (m, 1H), 6.95 – 6.89 (m, 2H), 4.73 (d, $J = 6.6$ Hz, 1H), 4.30 (d, $J = 5.7$ Hz, 1H), 3.50 (s, 3H), 3.34 (t, $J = 6.2$ Hz, 1H), 3.29 (s, 3H), 1.31 – 1.21 (m, 3H), 1.18 – 0.94 (m, 18H).

$^{13}\text{C NMR}$ (101 MHz, CDCl_3) δ 156.75, 135.04, 130.32, 121.50, 120.98, 120.40, 112.02, 111.99, 104.63, 56.36, 55.38, 49.11, 25.77, 17.99, 12.73.

HRMS (ESI): $m/z = \text{cald. for } \text{C}_{22}\text{H}_{35}\text{N}_2\text{O}_3\text{Si} [\text{M} + \text{H}]^+$: 403.2412, found: 403.2407; $[\text{M} + \text{Na}]^+$: 425.2231, found: 425.2224

5.5.14 2-(2,2-DIMETHOXY-1-(3-METHYL-1-PHENYL-1H-PYRAZOL-4-YL)ETHYL)MALONONITRILE (**13A**)



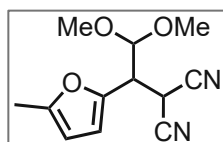
Starting from 2-((3-methyl-1-phenyl-1H-pyrazol-4-yl)methylene)malononitrile (**S 13**) and following the general procedure A. Purified by column chromatography (Alox N, pentane/EtOAc, 2.5:1, $R_f=0.39$). Pale yellow oil (27 mg, 88%).

$^1\text{H NMR}$ (500 MHz, CDCl_3) δ 8.07 (s, 1H), 7.72 – 7.62 (m, 2H), 7.50 – 7.41 (m, 2H), 7.32 – 7.25 (m, 1H), 4.61 (d, $J = 5.8$ Hz, 1H), 4.32 (d, $J = 4.8$ Hz, 1H), 3.52 (s, 3H), 3.53 – 3.47 (m, 1H), 3.39 (s, 3H), 2.40 (s, 3H).

$^{13}\text{C NMR}$ (126 MHz, CDCl_3) δ 149.85, 139.86, 129.55, 126.72, 126.29, 119.23, 113.79, 112.34, 112.22, 104.97, 56.74, 55.65, 40.67, 25.91, 12.01.

HRMS (ESI): $m/z = \text{cald. for } \text{C}_{17}\text{H}_{19}\text{N}_4\text{O}_2 [\text{M} + \text{H}]^+$: 311.1503, found: 311.1500

5.5.15 2-(2,2-DIMETHOXY-1-(5-METHYLFURAN-2-YL)ETHYL)
MALONONITRILE (**14A**)



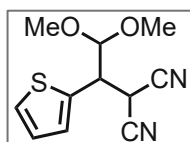
Starting from diethyl 2-((5-methylfuran-2-yl)methylene)malononitrile (**S 14**) and following the general procedure A. Purified by column chromatography (Alox N, pentane/EtOAc, 5:1, $R_f=0.32$). Colourless oil (18.1 mg, 78%).

$^1\text{H NMR}$ (500 MHz, CDCl_3) δ 6.35 (d, $J = 3.2$ Hz, 1H), 6.03 – 5.95 (m, 1H), 4.76 (d, $J = 7.0$ Hz, 1H), 4.29 (d, $J = 5.0$ Hz, 1H), 3.58 – 3.52 (m, 1H), 3.50 (s, 3H), 3.35 (s, 3H), 2.31 (d, $J = 1.1$ Hz, 3H).

$^{13}\text{C NMR}$ (101 MHz, CDCl_3) δ 153.43, 145.07, 111.86, 111.58, 111.18, 106.99, 103.25, 56.42, 55.04, 43.70, 24.65, 13.69.

HRMS (ESI): $m/z = \text{cald. for } \text{C}_{12}\text{H}_{15}\text{N}_2\text{O}_3 [\text{M} + \text{H}]^+$: 235.1077, found: 235.1072

5.5.16 2-(2,2-DIMETHOXY-1-(THIOPHEN-2-YL)ETHYL)
MALONONITRILE (**15A**)



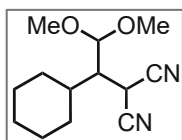
Starting from diethyl 2-(thiophen-2-ylmethylene)malononitrile (**S 15**) and following the general procedure A. Purified by column chromatography (Alox N, pentane/EtOAc, 5:1, $R_f=0.26$). Pale yellow oil (14.2 mg, 59%).

$^1\text{H NMR}$ (500 MHz, CDCl_3) δ 7.42 – 7.32 (m, 1H), 7.24 – 7.16 (m, 1H), 7.12 – 6.99 (m, 1H), 4.70 (d, $J = 5.7$ Hz, 1H), 4.35 (d, $J = 5.5$ Hz, 1H), 3.78 (t, $J = 5.6$ Hz, 1H), 3.54 (s, 3H), 3.41 (s, 3H).

$^{13}\text{C NMR}$ (101 MHz, CDCl_3) δ 134.66, 128.41, 127.37, 127.05, 112.01, 111.71, 104.83, 56.89, 55.87, 45.43, 26.36.

HRMS (ESI): $m/z = \text{cald. for } \text{C}_{11}\text{H}_{13}\text{N}_2\text{O}_2\text{S} [\text{M} + \text{H}]^+$: 237.0692, found: 237.0688

5.5.17 2-(1-CYCLOHEXYL-2,2-DIMETHOXYETHYL)
MALONONITRILE (**16A**)



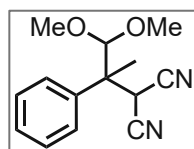
Starting from diethyl 2-(cyclohexylmethylene)malononitrile (**S 16**) and following the general procedure A. Purified by column chromatography (Alox N, pentane/Et₂O, 2:1, R_f=0.33). Colourless oil (15.2 mg, 64%).

¹H NMR (500 MHz, CDCl₃) δ 4.49 (d, *J* = 4.2 Hz, 1H), 4.20 (d, *J* = 2.7 Hz, 1H), 3.48 (s, 3H), 3.41 (s, 3H), 2.08 – 2.02 (m, 1H), 1.98 – 1.91 (m, 1H), 1.87 – 1.75 (m, 4H), 1.76 – 1.67 (m, 1H), 1.38 – 1.26 (m, 2H), 1.23 – 1.08 (m, 3H).

¹³C NMR (126 MHz, CDCl₃) δ 113.94, 112.84, 103.43, 56.96, 55.25, 49.41, 37.22, 30.97, 30.66, 26.17, 26.15, 20.26.

HRMS (ESI): *m/z* = calcd. for C₁₄H₁₇N₂O₂ [M + H]⁺: 237.1598, found: 237.1600, [M + Na]⁺: 259.1417, found: 259.1434

5.5.18 2-(1,1-DIMETHOXY-2-PHENYLPROPAN-2-YL)
MALONONITRILE (**17A**)



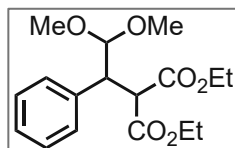
Starting from diethyl 2-(1-phenylethylidene)malononitrile (**S 17**) and following the general procedure A. Purified by column chromatography (Alox N, pentane/EtOAc, 5:1, R_f=0.46). Colourless oil (20.5 mg, 83%).

¹H NMR (500 MHz, CDCl₃) δ 7.55 – 7.49 (m, 2H), 7.44 – 7.39 (m, 2H), 7.39 – 7.34 (m, 1H), 4.64 (s, 1H), 4.36 (s, 1H), 3.54 (s, 3H), 3.42 (s, 3H), 1.72 (s, 3H).

¹³C NMR (126 MHz, CDCl₃) δ 137.27, 128.88, 128.65, 127.27, 112.19, 111.99, 109.29, 59.36, 58.96, 49.64, 32.36, 18.38.

HRMS (ESI): *m/z* = calcd. for C₁₄H₁₇N₂O₂ [M + H]⁺: 245.1285, found: 245.1278

5.5.19 DIETHYL 2-(2,2-DIMETHOXY-1-PHENYLETHYL) MALONATE (18A)



Starting from diethyl 2-benzylidenemalonate (**S 18**) and following the general procedure A. Purified by column chromatography (Alox N, pentane/EtOAc, 8:1, $R_f=0.35$). Colourless liquid (27.5 mg, 85%).

$^1\text{H NMR}$ (400 MHz, CDCl_3) δ 7.38 – 7.09 (m, 5H), 4.59 (d, $J = 6.0$ Hz, 1H), 4.27 – 4.08 (m, 2H), 3.93 – 3.81 (m, 3H), 3.80 – 3.67 (m, 1H), 3.34 (s, 3H), 3.24 (s, 3H), 1.26 (t, $J = 7.1$ Hz, 3H), 0.92 (t, $J = 7.1$ Hz, 3H).

$^{13}\text{C NMR}$ (126 MHz, CDCl_3) δ 168.41, 167.89, 137.39, 129.47, 128.24, 127.33, 106.56, 61.54, 61.31, 55.97, 54.61, 54.41, 48.52, 14.18, 13.78.

HRMS (ESI): $m/z =$ calcd. for $\text{C}_{17}\text{H}_{24}\text{O}_6\text{Na}$ $[\text{M} + \text{Na}]^+$: 347.1465, found: 347.1492; $[\text{2M} + \text{Na}]^+$: 671.3038, found: 671.3015; $[\text{M} + \text{K}]^+$: 363.1205, found: 363.1196

6 LIST OF FIGURES

Figure 1: Excitation by light of a component A from its ground state to an electronically excited state. The excited state then undergoes deactivation by chemical reaction and/or by radiative or non-radiative photophysical processes.	2
Figure 2: The Jablonski diagram. Illustration taken from the book Photochemistry and Photophysics by Balzani, Ceroni and Juris ^[5]	3
Figure 3: Schematic diagram of a reaction leading to different products that can be obtained by thermal vs. photochemical reaction. Illustration taken from the book Photochemistry and Photophysics by Balzani, Ceroni and Juris ^[5]	5
Figure 4: Molecular orbital representation of oxidative electron transfer from excited electron donor (A*) to electron acceptor (B) (redrawn from literature ^[9])	6
Figure 5: Molecular orbital representation of reductive electron transfer from electron donor (B) to excited electron acceptor (A*) (redrawn from literature ^[9])	6
Figure 6: Types of photochemical reactions. Figure taken from ^[12]	9
Figure 7: (A) General catalytic mechanism of photoredox catalysis. (B) Widely used photoredox catalysts and their photophysical properties. Figure taken from ^[12]	10
Figure 8: Commonly used molecules for direct photoexcitation. Figure taken from ^[14]	11
Figure 9: Nickel-catalysed cross-coupling process enabled by the photochemical activity of the 4-R-1,4-dihydropyridine. Reaction mixture was irradiated with LED $\lambda=405$ nm ^[17]	12
Figure 10: Enantioselective catalytic α -alkylation of aldehydes. Figure taken from ^[12]	12
Figure 11: Nicotine amide of NAD(P)H marked in green square and a Hantzsch ester on the right	13
Figure 12: Schematic illustration of transfer hydrogenation reactions	14
Figure 13: Photoredox C-H-arylation of amines. Graph taken from ^[43]	15
Figure 14: Examples from the literature using Hantzsch esters for C-C bond forming reactions ^[32, 44, 46]	15
Figure 15: General scheme of the radical transfer reaction	16
Figure 16: Acetalization of olefine substate and synthesis of aldehyde	16
Figure 17: The formation of acetal radicals <i>via</i> photoexcitation of Hantzsch esters	17

Figure 18: Examples for photochemical transformation using 4-dimethoxymethyl HE reagents ^[48-50]	17
Figure 19: Hantzsch ester synthesis.....	19
Figure 20: Mechanism of Hantzsch ester synthesis.....	19
Figure 21: The desired condensation product.....	20
Figure 22: Possible reaction mechanism of the ketene thioacetal formation.....	20
Figure 23: Dithianyl group introduction through silyl modification ^[52]	21
Figure 24: Dithianyl group introduction using 1,3-propane dithiol.....	21
Figure 25: UV-VIS absorbance spectrum of HE 2	22
Figure 26: UV-VIS absorption spectra of HE 2 (blue), S 1 (green) and a 1:1 mixture of HE 2 and S 1 (pink).....	23
Figure 27: Organo-photocatalysts tested for the reaction.....	25
Figure 28: Pictures of the reactor setup with water cooling (on the left) with fan cooling (on the right).....	26
Figure 29: Procedures for the exploration of the substrate scope for the transfer (thio)acetalization.....	30
Figure 30: Oxidation of the Hantzsch ester (HE 2).....	33
Figure 31: Cyclic voltammogram of HE 2 relative to Ag/AgCl electrode (3 M KCl);	34
Figure 32: Absorbance and emission spectrum of HE 2 and their intersection.....	35
Figure 33: Simplified redox potential diagram.....	36
Figure 34: Radical trapping experiment.....	37
Figure 35: GC-MS spectra of the radical trapping experiment.....	38
Figure 36: Result of the light on-off experiment.....	39
Figure 37: Proposed mechanistic pathways for the model reaction.....	40
Figure 38: Hantzsch esters as acetal group transfer-agents under photochemical conditions.....	41

7 LIST OF TABLES

Table 1: Reaction optimization under near UV light	24
Table 2: Optimization of the reaction conditions with a photocatalyst	25
Table 3: Evaluation of the LED light sources ($\lambda=365$ nm)	27
Table 4: Evaluation of the temperature control.....	27
Table 5: Evaluation of the reproducibility of the model reaction	28
Table 6: Evaluation of the reproducibility of the model reaction with 4CzIPN as a photocatalyst.....	29
Table 8: Substrate scope	31
Table 9: Comparison of the redox potentials	40

8 REFERENCES

1. De Marais, D.J., *Evolution. When did photosynthesis emerge on Earth?* Science, 2000. **289**(5485): p. 1703-1705.
2. Stirbet, A., et al., *Photosynthesis: basics, history and modelling.* Annals of Botany, 2019. **126**(4): p. 511-537.
3. Angelo Albini, M.F., *Handbook of Synthetic Photochemistry.* 2010: Wiley-VCH.
4. Yue, K., et al., *Trends and Opportunities in Organic Synthesis: Global State of Research Metrics and Advances in Precision, Efficiency, and Green Chemistry.* The Journal of Organic Chemistry, 2023. **88**(7): p. 4031-4035.
5. Vincenzo Balzani, P.C., Alberto Juris, *Photochemistry and Photophysics. Concepts, Research, Applications.* 2014: John Wiley & Sons.
6. Roth, H.D., *The Beginnings of Organic Photochemistry.* Angewandte Chemie International Edition in English, 1989. **28**(9): p. 1193-1207.
7. Jaffe, H.H. and A.L. Miller, *The fates of electronic excitation energy.* Journal of Chemical Education, 1966. **43**(9): p. 469-473.
8. Baba, M., *Intersystem Crossing in the $1n\pi^*$ and $1\pi\pi^*$ States.* The Journal of Physical Chemistry A, 2011. **115**(34): p. 9514-9519.
9. Wardle, B., *Principles and applications of photochemistry.* 2009: John Wiley & Sons.
10. Grampp, G., *Fundamentals of photoinduced electron transfer.* Berichte der Bunsengesellschaft für physikalische Chemie, 1994. **98**(10): p. 1349-1349.
11. Prier, C.K., D.A. Rankic, and D.W.C. MacMillan, *Visible Light Photoredox Catalysis with Transition Metal Complexes: Applications in Organic Synthesis.* Chemical Reviews, 2013. **113**(7): p. 5322-5363.
12. Sumida, Y. and H. Ohmiya, *Direct excitation strategy for radical generation in organic synthesis.* Chemical Society Reviews, 2021. **50**(11): p. 6320-6332.
13. Romero, N.A. and D.A. Nicewicz, *Organic Photoredox Catalysis.* Chemical Reviews, 2016. **116**(17): p. 10075-10166.
14. He, X.K., et al., *Direct Photoexcitation of Benzothiazolines: Acyl Radical Generation and Application to Access Heterocycles.* Molecules, 2021. **26**(22).
15. Schmidt, V.A., et al., *Site-Selective Aliphatic C–H Bromination Using N-Bromoamides and Visible Light.* Journal of the American Chemical Society, 2014. **136**(41): p. 14389-14392.
16. Czaplyski, W.L., C.G. Na, and E.J. Alexanian, *C–H Xanthylation: A Synthetic Platform for Alkane Functionalization.* Journal of the American Chemical Society, 2016. **138**(42): p. 13854-13857.
17. Buzzetti, L., et al., *Radical-Based C-C Bond-Forming Processes Enabled by the Photoexcitation of 4-Alkyl-1,4-dihydropyridines.* Angew Chem Int Ed Engl, 2017. **56**(47): p. 15039-15043.
18. Mulliken, R.S., *Structures of Complexes Formed by Halogen Molecules with Aromatic and with Oxygenated Solvents*1. Journal of the American Chemical Society, 1950. **72**(1): p. 600-608.
19. Crisenza, G.E.M., D. Mazzarella, and P. Melchiorre, *Synthetic Methods Driven by the Photoactivity of Electron Donor–Acceptor Complexes.* Journal of the American Chemical Society, 2020. **142**(12): p. 5461-5476.
20. Arceo, E., et al., *Photochemical activity of a key donor–acceptor complex can drive stereoselective catalytic α -alkylation of aldehydes.* Nature Chemistry, 2013. **5**(9): p. 750-756.
21. Hantzsch, A., *Condensationsprodukte aus Aldehydammoniak und ketonartigen Verbindungen.* Berichte der deutschen chemischen Gesellschaft, 1881. **14**(2): p. 1637-1638.
22. Wang, X., et al., *Cofactor NAD(P)H Regeneration Inspired by Heterogeneous Pathways.* Chem, 2017. **2**(5): p. 621-654.

23. Sharma, V.K., J.M. Hutchison, and A.M. Allgeier, *Redox Biocatalysis: Quantitative Comparisons of Nicotinamide Cofactor Regeneration Methods*. ChemSusChem, 2022. **15**(22): p. 1-24.
24. Huang, X., et al., *Photoinduced chemomimetic biocatalysis for enantioselective intermolecular radical conjugate addition*. Nature Catalysis, 2022. **5**(7): p. 586-593.
25. Zheng, C. and S.-L. You, *Transfer hydrogenation with Hantzsch esters and related organic hydride donors*. Chemical Society Reviews, 2012. **41**(6): p. 2498-2518.
26. Cui, X. and K. Burgess, *Catalytic Homogeneous Asymmetric Hydrogenations of Largely Unfunctionalized Alkenes*. Chemical Reviews, 2005. **105**(9): p. 3272-3296.
27. Jäkel, C. and R. Paciello, *High-Throughput and Parallel Screening Methods in Asymmetric Hydrogenation*. Chemical Reviews, 2006. **106**(7): p. 2912-2942.
28. Cortez, N.A., et al., *Ruthenium(II) and rhodium(III) catalyzed asymmetric transfer hydrogenation (ATH) of acetophenone in isopropanol and in aqueous sodium formate using new chiral substituted aromatic monosulfonamide ligands derived from (1R,2R)-diaminocyclohexane*. Tetrahedron: Asymmetry, 2008. **19**(11): p. 1304-1309.
29. Wang, C., X. Wu, and J. Xiao, *Broader, Greener, and More Efficient: Recent Advances in Asymmetric Transfer Hydrogenation*. Chemistry – An Asian Journal, 2008. **3**(10): p. 1750-1770.
30. Ruhland, K., *Transition-Metal-Mediated Cleavage and Activation of C–C Single Bonds*. European Journal of Organic Chemistry, 2012. **2012**(14): p. 2683-2706.
31. Nakao, Y., *Nickel/Lewis Acid-Catalyzed Carbocyanation of Unsaturated Compounds*. Bulletin of the Chemical Society of Japan, 2012. **85**(7): p. 731-745.
32. Nakajima, K., et al., *Visible-Light-Mediated Aromatic Substitution Reactions of Cyanoarenes with 4-Alkyl-1,4-dihydropyridines through Double Carbon–Carbon Bond Cleavage*. ChemCatChem, 2016. **8**(6): p. 1028-1032.
33. Xuan, J. and W.-J. Xiao, *Visible-Light Photoredox Catalysis*. Angewandte Chemie International Edition, 2012. **51**(28): p. 6828-6838.
34. Koike, T. and M. Akita, *Visible-Light-Induced Photoredox Catalysis: An Easy Access to Green Radical Chemistry*. Synlett, 2013. **24**(19): p. 2492-2505.
35. Schmittel, M. and A. Burghart, *Understanding Reactivity Patterns of Radical Cations*. Angewandte Chemie International Edition in English, 1997. **36**(23): p. 2550-2589.
36. Mella, M., et al., *New synthetic methods via radical cation fragmentation*. Chemical Society Reviews, 1998. **27**(1): p. 81-89.
37. Baciocchi, E., M. Bietti, and O. Lanzalunga, *Fragmentation reactions of radical cations*. Journal of Physical Organic Chemistry, 2006. **19**(8-9): p. 467-478.
38. Houmam, A., *Electron Transfer Initiated Reactions: Bond Formation and Bond Dissociation*. Chemical Reviews, 2008. **108**(7): p. 2180-2237.
39. Cai, S., et al., *Visible-Light-Promoted C–C Bond Cleavage: Photocatalytic Generation of Iminium Ions and Amino Radicals*. Angewandte Chemie International Edition, 2012. **51**(32): p. 8050-8053.
40. Zhao, Y., et al., *Visible-light photo-catalytic C–C bond cleavages: preparations of N,N-dialkylformamides from 1,2-vicinal diamines*. Tetrahedron, 2013. **69**(38): p. 8129-8131.
41. Laha, J.K., K.S.S. Tummalapalli, and A. Gupta, *Transition-Metal-Free Tandem Oxidative Removal of Benzylic Methylene Group by C–C and C–N Bond Cleavage Followed by Intramolecular New Aryl C–N Bond Formation under Radical Conditions*. Organic Letters, 2014. **16**(17): p. 4392-4395.
42. Ohashi, M. and K. Miyake, *Photochemical reactions of p-dicyanobenzene with primary and secondary amines*. Chemistry Letters, 2006. **6**(6): p. 615-616.
43. McNally, A., C.K. Prier, and D.W.C. MacMillan, *Discovery of an α -Amino C–H Arylation Reaction Using the Strategy of Accelerated Serendipity*. Science, 2011. **334**(6059): p. 1114-1117.

44. Cardinale, L., M.O. Konev, and A. Jacobi von Wangelin, *Photoredox-Catalyzed Addition of Carbamoyl Radicals to Olefins: A 1,4-Dihydropyridine Approach*. Chemistry – A European Journal, 2020. **26**(37): p. 8239-8243.
45. Cardinale, L., et al., *Photoredox-Catalyzed Synthesis of α -Amino Acid Amides by Imine Carbamoylation*. Organic Letters, 2022. **24**(2): p. 506-510.
46. Pálvölgyi, Á.M., et al., *Photocatalyst-free hydroacylations of electron-poor alkenes and enones under visible-light irradiation*. Organic & Biomolecular Chemistry, 2022. **20**(36): p. 7245-7249.
47. Wang, P.-Z., J.-R. Chen, and W.-J. Xiao, *Hantzsch esters: an emerging versatile class of reagents in photoredox catalyzed organic synthesis*. Organic & Biomolecular Chemistry, 2019. **17**(29): p. 6936-6951.
48. Wang, Z.-J., et al., *Desulfonative photoredox alkylation of N-heteroaryl sulfones – an acid-free approach for substituted heteroarene synthesis*. Chemical Science, 2019. **10**(16): p. 4389-4393.
49. Gu, F.J., et al., *Substituted Hantzsch Esters as Versatile Radical Reservoirs in Photoredox Reactions*. Advanced Synthesis & Catalysis, 2018. **360**(5): p. 925-931.
50. Chen, C.C. and J. Waser, *One-Pot, Three-Component Arylalkynyl Sulfone Synthesis*. Organic Letters, 2015. **17**(3): p. 736-739.
51. Meyers, A. and R.C. Strickland, *Synthesis and properties of 2-(2-cyanoethylidene)-1,3-dithiane and its isomeric ketene thioacetal*. The Journal of Organic Chemistry, 1972. **37**(16): p. 2579-2583.
52. Soderquist, J.A. and E.I. Miranda, *A rapid, efficient and selective conversion of aldehydes and acetals to their 1,3-dithiane derivatives with 2,2-dimethyl-2-sila-1,3-dithiane*. Tetrahedron Letters, 1986. **27**(52): p. 6305-6306.
53. Wu, Q.-Y., et al., *Radical alkylation of para-quinone methides with 4-substituted Hantzsch esters/nitriles via organic photoredox catalysis*. Organic & Biomolecular Chemistry, 2018. **16**(35): p. 6391-6394.
54. Svejstrup, T.D., et al., *Effects of Light Intensity and Reaction Temperature on Photoreactions in Commercial Photoreactors*. ChemPhotoChem, 2021. **5**(9): p. 808-814.
55. Buzzetti, L., G.E.M. Crisenza, and P. Melchiorre, *Mechanistic Studies in Photocatalysis*. Angewandte Chemie International Edition, 2019. **58**(12): p. 3730-3747.
56. Kazuhiko, M., I. Munehiro, and O. Yoshio, *Dual Regioselectivity in the Photoallylation of Electron-Deficient Alkenes by Allylic Silanes*. Chemistry Letters, 1988. **17**(9): p. 1507-1510.
57. Wieber, M. and M. Schmidt, *Über die Umsetzung von Dimethyldichlorsilan, -german und -stannan mit Propan-1,3-dithiol*. Journal of Organometallic Chemistry, 1964. **1**(4): p. 336-339.
58. Meyers, A.I. and R.C. Strickland, *Synthesis and properties of 2-(2-cyanoethylidene)-1,3-dithiane and its isomeric ketene thioacetal*. The Journal of Organic Chemistry, 1972. **37**(16): p. 2579-2583.
59. Dalessandro, E.V., et al., *Mechanism of the Piperidine-Catalyzed Knoevenagel Condensation Reaction in Methanol: The Role of Iminium and Enolate Ions*. The Journal of Physical Chemistry B, 2017. **121**(20): p. 5300-5307.